Ultra-deep 31.0–50.3 GHz spectral survey of IRC+10216[⋆,⋆⋆]

J. R. Pardo[1], J. Cernicharo[1], B. Tercero[2], C. Cabezas[1], C. Bermúdez[1], M. Agúndez[1], J. D. Gallego[2], F. Tercero[2], M. Gómez-Garrido[2], P. de Vicente[2], and J. A. López-Pérez[2]

[1] Consejo Superior de Investigaciones Científicas, Instituto de Física Fundamental, Serrano 123, 28006 Madrid, Spain
e-mail: jr.pardo@csic.es
[2] Instituto Geográfico Nacional, Centro de Desarrollos Tecnológicos, Observatorio de Yebes, Apartado 148, 19080 Yebes, Spain

ABSTRACT

Context. The carbon-rich envelope of the asymptotic giant branch star CW Leo, IRC+10216, is one of the richest molecular sources in the sky. Available spectral surveys below 51 GHz are more than 25 years old, and new work is needed.
Aims. Characterizing the rich molecular content of this source, specially for heavy species, requires carrying out very sensitive spectral surveys at low frequencies. In particular, we have achieved an rms in the range 0.2−0.6 mK per MHz.
Methods. Long Q band (31.0−50.3 GHz) single-dish integrations were carried out with the Yebes-40m telescope using specifically built receivers. The most recent line catalogs were used to identify the lines.
Results. The data contain 652 spectral features, corresponding to 713 transitions from 81 species (we count the isomers, isotopologs, and ortho/para species separately). Only 57 unidentified lines remain with signal-to-noise ratios ≥3. Some new species and/or vibrational modes have been discovered for the first time with this survey.
Conclusions. This IRC+10216 spectral survey is by far the most sensitive survey carried out to date in the Q band. It therefore provides the most complete view of IRC+10216 from 31.0 to 50.3 GHz, giving unique information about its molecular content, especially for heavy species. Rotational diagrams built from the data provide valuable information about the physical conditions and chemical content of this circumstellar envelope.

Key words. line: identification – stars: AGB and post-AGB – stars: carbon – stars: individual: IRC+10216 – radio lines: stars – surveys

1. Introduction

The combination of proximity (123 ± 14 pc from the Sun; Groenewegen et al. 2012) and high mass-loss rate ($\dot{M} = (2−4) \times 10^{-5} \, M_\odot \, \text{yr}^{-1}$; Cernicharo et al. 2015; Guélin et al. 2018) makes IRC+10216 the main stellar target for molecule hunting in space (Cernicharo et al. 2000). In this context, the largest work at millimeter wavelengths (4.3−1.0 mm) has been carried out with the 30 meter diameter radiotelescope from the Institut de Radiostronomie Millimétrique (IRAM-30m), located in Sierra Nevada, Spain. Accumulated data achieved during more than three decades are now in their final phase of analysis for publication (Cernicharo et al., in prep.). In order to complement these data at the longer end of the millimeter range (6.0−9.7 mm, or 31.0 to 50.3 GHz in frequency), which is especially important for the detection of heavy molecules, we decided to perform an extremely deep integration in the so-called Q band toward IRC+10216 and several other stellar sources that are known for their molecular richness. For this work, it was important to have access to a large antenna in order to keep angular resolutions similar to those provided by the IRAM-30m (but here at wavelengths 1.4 to 10 times larger), the

most recent receivers with very broad instantaneous bands to reduce telescope time for a given rms goal, and high spectral resolutions to allow for degradation if desired.

The importance of sensitive surveys for understanding the rich molecular complexity found in the Universe, eventually leading to the appearance of life, is unquestionable and has made much progress in recent years due to two key factors. On one hand, the rapid and strong increase in the instantaneous bands of receivers, which allows accumulating long integration times over large frequency bands because short-spaced frequency tunings are no longer necessary. On the other hand, large interferometers now in operation, such as the Atacama Large Millimeter Array (ALMA) or thw NOrthern Extended Millimeter Array (NOEMA), allow exploring the sources with rich molecular content at narrower angular scales, thus providing a new molecular view of them because some molecular species, especially for stellar sources, appear only in the innermost regions of their envelopes.

The spectral region below the atmospheric 60 GHz O_2 spin-rotation band generally lacks coverage by the most important millimeter wave single-dish telescopes or interferometers. In addition, due to the wavelength, large antennas are needed to keep a reasonably coupling to stellar sources. As a consequence, available spectral surveys of IRC+10216 in the Q band are more than 25 years old (Kawaguchi et al. 1995). This has motivated our work, in which we present a great improvement with respect to the past. The step forward is not only due to technical reasons related to the observational capabilities themselves, but also to a continuous effort of extending the spectroscopic databases with
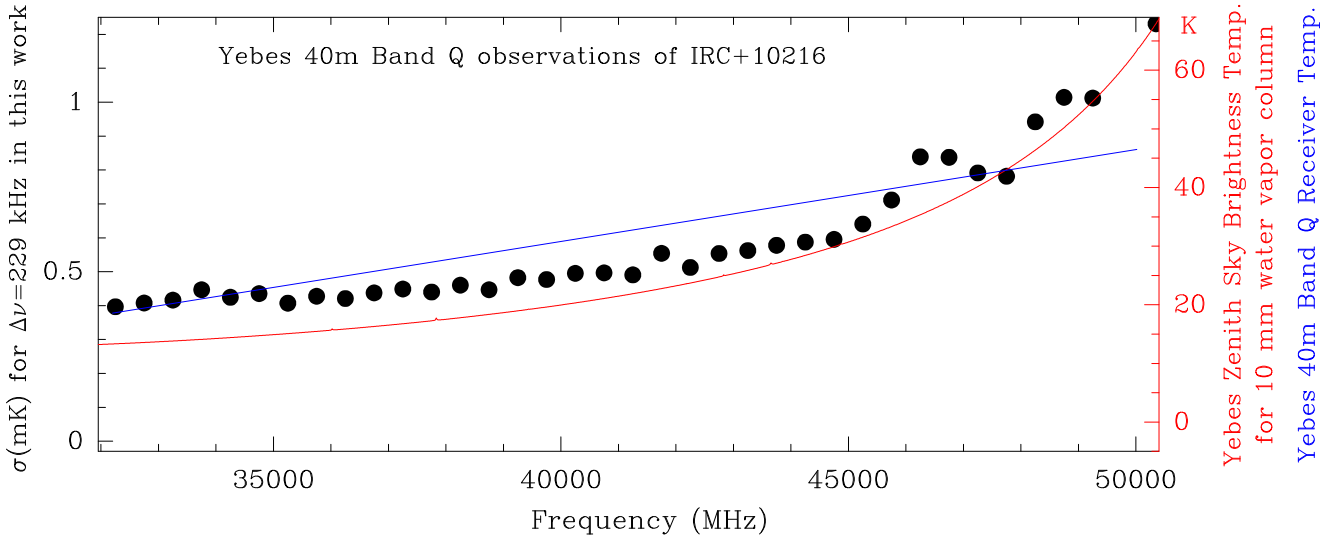

Fig. 1. Noise level in the spectra presented in this work at their final resolution (see Sect. 3) and typical atmospheric brightness temperature and average receiver temperature across the band.

the latest laboratory and theoretical results. The observations are described in Sect. 2. The systematic procedure for data reduction, line identification, assignment and fitting is described in Sect. 3. We present the results in Sect. 4, although some material is available only in electronic from. The procedure for line identification and handling this large amount of information is described in Sect. 5. A summary stressing the legacy importance of the results obtained in this work, in the framework of our knowledge of the physical conditions and chemistry of IRC+10216, is finally given in Sect. 6.

2. Observations

This IRC+10216 31.0−50.3 GHz spectral survey was carried out in several runs from May 2019 to February 2020, and in April 2021, with the 40-meter antenna of Yebes Observatory (IGN, Spain), hereafter Yebes-40m, after several improvements in its equipment funded by the Nanocosmos project[1]. This large antenna now provides a main-beam efficiency from 0.6 at 31 GHz to 0.43 at 50 GHz and a beam size in the range 36−56″ for these frequencies. Although the experimental setup is described in detail in a separate technical paper (Tercero et al. 2021), the most relevant information for this work is the use of a receiver consisting of two HEMT cold amplifiers covering the 31.0−50.3 GHz band with horizontal and vertical polarizations. The receiver temperature ranges from 22 K at 31 GHz to 42 K at 50 GHz. The backends are 16×2.5 GHz fast-Fourier transform spectrometers (FFTS), with a primary spectral resolution of 38.1 kHz (later smoothed in the data reduction for this work). They provide the whole coverage of the observed band.

The observing mode was position switching with an off position at 300″ in azimuth. The reference position used for IRC+10216 was J2000 RA 09:47:57.36 Dec +13:16:44.4. The half-power beam width (HPBW) of the antenna at 39.2 GHz is 45″. Pointing corrections were obtained by observing the SiO masers of R Leo, and errors were always within 2−3″. The intensity scale of the first-calibrated spectra is an antenna temperature (T_A^*) corrected for atmospheric absorption using the ATM package (Cernicharo 1985; Pardo et al. 2001). A conversion into

main-beam temperature (T_{MB}) was made in order to generate the rotational diagrams. Calibration uncertainties are estimated to be within 10%. More details about the observational procedure can be found in Pardo et al. (2020).

3. Data reduction and analysis

The GILDAS package[2] was used to add up the raw spectra provided by the telescope calibration software, to fit individual baselines in the different FFTS sections, and to stitch all these sections into a final spectrum using the appropriate weights according to system temperatures and integration times of each individual scan. If necessary, additional baselines were fit to narrow sections of the data, but these interventions were kept to a strict minimum. The resulting spectrum was smoothed to a resolution of 0.229 MHz, for which the sensitivity ranges from ∼0.4 to 1.2 mK in the surveyed frequency range (see Fig. 1). The average data noise every 500 MHz shown in Fig. 1 is the basis for a first automatic procedure, which determines which observed spectral features are above the 3σ level. A second check is done by hand to spot features that were missed in the first step. When the detected spectral features were well established, the next step was to assign them to molecular lines. For this task, we relied upon the latest version of the MADEX line catalog (Cernicharo et al. 2012), which has up to 6150 molecular species and 23.5 million transitions. We proceeded in several steps. As part of the automatic procedures, there was first a cross-check between the data and the catalog to assign as many lines as possible. Second, all the assignments were confirmed by hand in order to eliminate errors and to identify blended lines from different species, lines spread due to hyperfine structure, etc. A third step consisted of assigning lines that were not present in the catalog to new species, isotopologs, or vibrational levels. This step resulted in the discovery of the ν_{19} vibrational mode of HC$_9$N (Pardo et al. 2020) for the first time in space and of the Mg-containing carbon chains MgC$_5$N and MgC$_6$H (Pardo et al. 2021). This careful work has allowed us to identify 93% of all lines present in the data. In addition, features at the 2−3σ level with a linewidth compatible with the ±14.5 km s^{-1} typical of the

source were also individually checked by hand. This resulted in additional assignments, mainly of ^{13}C substitutions of HC_7N.

The overall summary of the identification work described in this section is the following: 652 spectral features belonging to 713 identified lines and 57 unidentified lines (U-lines). An overview is given in Table 1. The details of the results of individual fits to all lines obtained using the SHELL method implemented in the GILDAS software are listed in Table A.1 and the remaining U-lines in Table 2. The final spectra presented in this paper (Figs. 2, and A.1–A.39) improve the sensitivity of those presented in the previous work conducted with the Nobeyama 45m telescope (Kawaguchi et al. 1995) in a similar frequency range by a factor of ≈ 10. They label 132 lines and report 33 U-lines. Of these U-lines, we were able to label 22 with the spectroscopic data available today (they correspond to C_8H, C_6H^- C_5N^-, C_6H, HC_9N, and HC_7N ν_{15}), 6 are spurious features as they are not present in our data, and 5 are still U-lines for us in 2021. The strongest observed feature (at 14σ in our data) that still remains unidentified stands at 41 712 MHz.

4. Results

The detected lines can be divided into different families of carriers. We present the results for each of these separately.

4.1. Cyanopolyynes

This molecular family, $HC_{2n+1}N$, dominates the millimeter wave spectrum of this source, as happens with other C-rich evolved stars such as CRL 618. In IRC+10216, up to 304 lines (43% of all detected lines in the Q band) belong to this family, which comprises HCN, HC_3N, HC_5N, HC_7N, and HC_9N in their main species, isotopic substitutions, vibrationally excited states, together with a few isomers. The upper panels in Figs. 3 and 4 provide a quick view of all lines from this family in this work. The difference with respect to Kawaguchi et al. (1995) is quite large because they were unable to detect isotopic substitutions of HC_5N or the vibrational states of HC_5N, HC_7N, and HC_9N. Sometimes, ν_{11} lines of HC_5N are present in their data but are labeled U, probably due to the lack of information in line catalogs available in 1995. The alternative single and triple C-bond is the dominant chemical feature in this source because most radicals, anions, and metal-bearing species are carbon chains of this type.

Although there are no lines from the main rotational ladder of HCN in the Q band, three l-doubling transitions from the $\nu_2 = 1$ vibrational state are present in the data ($J = 12-12$, $13-13$, and $14-14$). The upper energy levels of these transitions lie between 1300 and 1500 K, and therefore, the signal detected arises from much closer to the photosphere of CW Leo than most lines in this work. They are also more narrow. Although this is the first Q band detection in IRC+10216 of HCN l-doubling lines, higher-J lines have previously been reported (Cernicharo et al. 2011).

4.2. Carbon-chain radicals

The list of radicals detected that are related with the cyanopolyynes is also long: C_3H, C_4H, C_5H, C_6H, C_7H, C_8H, C_3N ($^{13}CCCN$, $C^{13}CCN$, $CC^{13}CN$), and C_5N. They are responsible for a total of 167 lines or 23% of all detected and labeled spectral lines in this work. Their open structure causes several configurations to lie close in energy, and hyperfine structure is also common for them. C_3H presents six hyperfine compo-

nents (two of them blended) in its ground-vibrational state, from 32 617 to 32 668 MHz. Another set of hyperfine components from 44 857 to 44 939 GHz, corresponding to the ν_4 vibrational mode (at 42.4 K), is not detected in the data. C_4H presents a total of nine doublets corresponding to its ground-, ν_7, and $2\nu_7$ vibrational states. C_5H presents four doublets for each one of the lowest states: $^2\Pi_{3/2}$ (not resolved) and $^2\Pi_{1/2}$ (resolved). C_6H is detected as resolved doublets from its $^2\Pi_{3/2}$ and $^2\Pi_{1/2}$ states, and other lines from the vibronic states $^2\Sigma^-$, $^2\Delta_{3/2}$, and $^2\Delta_{5/2}$ belonging to the ν_{11} vibrational state are also detected.

The total number of lines from C_6H is 56, which is the largest number in this family. Finally, C_7H and C_8H also display doublets in the states $^2\Pi_{3/2}$ and $^2\Pi_{1/2}$. Only the last one is resolved in both cases, although the lowest energy state is $^2\Pi_{1/2}$ for C_7H and $^2\Pi_{3/2}$ for C_8H.

The total number of spectral features of C_7H and C_8H detected is 23 and 31, respectively, with a counterpart of 33 and 46, respectively, rotational transitions.

Other radicals detected in this family are C_3N (two doublets at 39 571/39 590 and 49 466/49 485 MHz), the ^{13}C isotopic substitutions of it (marginal), and C_5N through two extremely weak doublets at 39 280/39 291 and 42 086/42 097 MHz. For a graphic summary of all lines from carbon-chain radicals, see the second panels of Figs. 3 and 4.

4.3. Anions

So far, IRC+10216 is the only circumstellar environnment in which anions have been detected. The survey presented in this paper provided a good opportunity for detecting heavy linear anions, and the results have confirmed these expectations: C_5N^-, C_6H^-, and C_8H^- are detected through 6, 8 and 13 lines, respectively. The lighter anion C_4H^- might be present, but its two transitions at 37 239.41 and 46 549.16 MHz are very close in frequency with the lines of $HCC^{13}CCCN$ and $HCCC^{13}CCN$ for the first and with HC_9N ν_{19} for the second, to the point of preventing a confirmation of its detection. The same holds for the C_3N^- line at 48 515.87 (blended with a strong C_6H line). The other line of C_3N^- at 38 812.79 MHz is not seen. This result is compatible with its low abundance that was revealed from its discovery in this source at higher frequencies (Thaddeus et al. 2008). C_5N^- and C_6H^- are expected (and confirmed) to display the strongest lines of the anions in this survey. A graphic summary of all lines from anions can be found on the third panel of Figs. 3 and 4.

4.4. Si-bearing species

The only oxygen-bearing species detected in our line survey is SiO. The $J = 1-0$ transition is detected for the main isotopolog as well as for ^{29}SiO and ^{30}SiO. On the other hand, $Si^{17}O$ at 41 794.658 MHz and $Si^{18}O$ at 40 352.771 might be there, but their detection is still marginal at the actual noise level.

Another Si-bearing molecule with only one rotational transition in this range ($J = 1-0$) is SiS. It has been detected for its main isotopolog as well as for ^{29}SiS, ^{30}SiS, $Si^{33}S$, and $Si^{34}S$.

The cyclic C_{2v} molecule SiC_2 has two lines that are strong enough for detection in the surveyed frequency range. Except for $^{29}SiC_2$ (one detected line), all other substitutions (SiC_2, $^{30}SiC_2$, and $^{13}CSiC$) exhibit two detected lines here.

The linear molecule SiC_4 has six rotational transitions in the surveyed frequency range (from $J = 11-10$ to $J = 16-15$). The multiple possible isotopic substitutions make it a candidate for a large number of lines in this source, but only $^{29}SiC_4$ can be confirmed as detected here. Five of its individual six rotational

Table 1. Molecules and total number of spectral features (N) and lines (L) detected in this work for each one of them. μ is the molecule electric dipole moment in Debyes (1 Debye = 3.33564×10^{-30} C m).

Molecule	μ	N/L	References for spectroscopy	Molecule	μ	N/L	References for spectroscopy
HCN	2.985	3/3	Zelinger et al. (2003), Ebenstein & Muenter (1984)	HC_3N	3.732	8/10	Mbosei et al. (2000), Thorwirth et al. (2000)
$H^{13}CCCN$	3.732	2/2	Creswell et al. (1977), Mallinson & de Zafra (1978), Thorwirth et al. (2001)	$HC^{13}CCN$	3.732	2/2	Same as $H^{13}CCCN$.
$HCC^{13}CN$	3.732	2/2	Same as $H^{13}CCCN$.	HCCNC	2.957	2/2	Guarnieri et al. (1992), Gripp et al. (2000)
$HCCN^{13}C$	2.957	2/2	Same as HCCNC	HNCCC	5.665	2/2	Kawaguchi et al. (1992), Hirahara et al. (1993), Botschwina et al. (1992)
HC_5N	4.330	20/22	Bizzocchi et al. (2004), Alexander et al. (1976)	$H^{13}CCCCCN$	4.330	8/8	Same as HC_5N.
$HC^{13}CCCCN$	4.330	8/8	Same as HC_5N.	$HCC^{13}CCCN$	4.330	7/7	Same as HC_5N.
$HCCC^{13}CCN$	4.330	7/7	Same as HC_5N.	$HCCCC^{13}CN$	4.330	8/8	Same as HC_5N.
HC_7N	4.820	72/74	McCarthy et al. (2000), Degli Esposti & Bizzocchi (2004), Botschwina et al. (1997)	$H^{13}CCCCCCCN$	4.820	10/11	McCarthy et al. (2000), Botschwina et al. (1997)
$HC^{13}CCCCCN$	4.820	8/8	Same as $H^{13}CCCCCCCN$	$HCC^{13}CCCCN$	4.820	10/10	Same as $H^{13}CCCCCCCN$
$HCCC^{13}CCCN$	4.820	10/10	Same as $H^{13}CCCCCCCN$	$HCCCC^{13}CCCN$	4.820	6/6	Same as $H^{13}CCCCCCCN$
$HCCCCC^{13}CCN$	4.820	11/11	Same as $H^{13}CCCCCCCN$	$HCCCCCC^{13}CN$	4.820	9/9	Same as $H^{13}CCCCCCCN$
HC_9N	5.200	80/80	McCarthy et al. (2000), Botschwina et al. (1997), Pardo et al. (2020)	HCCN	3.600	1/1	Allen et al. (2001), Aoki & Ikuta (1993)
$l\text{-}HC_4N$	4.330	6/6	Tang et al. (1999), Ikuta et al. (2000)	$o\text{-}H_2C_4$	4.457	6/6	Killian et al. (1990), Oswald & Botschwina (1995)
$p\text{-}H_2C_4$	4.457	4/5	Killian et al. (1990), Oswald & Botschwina (1995)	$o\text{-}H_2C_3$	4.100	2/2	Vrtilek et al. (1990)
$p\text{-}H_2C_3$	4.100	1/1	Vrtilek et al. (1990)	C_3H	3.550	6/6	Yamamoto et al. (1990a), Gottlieb et al. (1985), Kaifu et al. (2004), Woon (1995)
C_4H	2.100	18/19	Guélin et al. (1982), Gottlieb et al. (1983), Chen et al. (1995), Oyama et al. (2020)	C_5H	4.881	12/16	McCarthy et al. (1999), Woon (1995)
C_6H	5.540	56/56	Linnartz et al. (1999), Woon (1995)	C_7H	5.945	23/33	McCarthy et al. (1997), Woon (1995)
C_8H	6.500	31/46	McCarthy et al. (1996), McCarthy et al. (1999)	C_3N	2.850	4/4	McCarthy et al. (1995), Guélin et al. (1982), Gottlieb et al. (1983)
$CC^{13}CN$	2.850	4/6	McCarthy et al. (1995), McCarthy et al. (2003)	$C^{13}CCN$	2.850	4/4	Same as $CC^{13}CN$
$^{13}CCCN$	2.850	5/6	Same as $CC^{13}CN$	C_5N	3.385	4/4	Kasai et al. (1997), Botschwina (1996)
C_5N^-	5.200	6/6	Cernicharo et al. (2008)	C_6H^-	8.200	7/8	McCarthy et al. (2006), Blanksby et al. (2001)
C_8H^-	10.400	13/13	Gupta et al. (2007), Blanksby et al. (2001)	$c\text{-}C_3H_2$ (ortho)	3.430	2/2	Thaddeus et al. (1985), Bogey et al. (1986), Vrtilek et al. (1987), Spezzano et al. (2012), Kanata et al. (1987)

Table 1. continued.

Molecule	μ	N/L	References for spectroscopy	Molecule	μ	N/L	References for spectroscopy
c-C$_3$H$_2$ (para)	3.430	2/2	Same as c-C$_3$H$_2$ (ortho)	SiS	1.735	1/1	Müller et al. (2007), Tiemann et al. (1972), Sanz et al. (2003)
^{29}SiS	1.735	1/1	Same as $^{(28)}$SiS.	^{30}SiS	1.735	1/1	Same as $^{(28)}$SiS.
Si^{33}S	1.735	1/1	Same as $^{(28)}$SiS.	Si^{34}S	1.735	1/1	Same as $^{(28)}$SiS.
SiO	3.098	1/1	Manson et al. (1977), Mollaaghababa et al. (1991), Sanz et al. (2003), Cho & Saito (1998), Raymonda et al. (1970)	^{29}SiO	3.098	1/1	Same as $^{(28)}$SiO.
^{30}SiO	3.098	1/1	Same as $^{(28)}$SiO.	Si^{17}O	3.098	1/1	Same as $^{(28)}$SiO.
SiC$_2$	2.393	2/2	Gottlieb et al. (1989), Suenram et al. (1989)	Si^{13}CC	2.393	2/2	Cernicharo et al. (1991)
^{29}SiC$_2$	2.393	1/1	Suenram et al. (1989), Cernicharo et al. (1991), Kokkin et al. (2011)	^{30}SiC$_2$	2.393	2/2	Same as ^{29}SiC$_2$
SiC$_4$	6.420	6/6	Ohishi et al. (1989), Gordon et al. (2000)	^{29}SiC$_4$	6.420	5/5	Same as ^{29}SiC$_4$
SiC$_6$	8.220	7/7	Gordon et al. (2000)	CS	1.958	1/1	Gottlieb et al. (2003), Winnewisser & Cook (1968)
^{13}CS	1.958	1/1	Same as CS.	C^{33}S	1.958	1/1	Same as CS.
C^{34}S	1.958	1/1	Same as CS.	C^{36}S	1.958	1/1	Same as CS.
CCS	2.855	4/4	Saito et al. (1987), Yamamoto et al. (1990b), Lovas et al. (1992), Lee (1997)	C$_3$S	3.704	3/3	Yamamoto et al. (1987), Tang & Saito (1995), Lovas et al. (1992), Ohshima & Endo (1992), Suenram & Lovas (1994)
NaCN	8.850	7/8	Van Vaals et al. (1984), Halfen & Ziurys (2011)	MgCN	5.150	2/2	Anderson et al. (1994), Hirano et al. (2002)
MgNC	5.308	4/4	Kawaguchi et al. (1993), Steimle & Bousquet (2001)	MgC$_3$N	6.250	14/14	Cernicharo et al. (2019)
MgC$_5$N	7.300	20/30	Pardo et al. (2021)	MgC$_4$H	2.100	10/10	Cernicharo et al. (2019)
MgC$_6$H	2.500	23/30	Pardo et al. (2021)	CH$_3$CN	3.925	2/3	Pavone et al. (1990), Cazzoli & Puzzarini (2006), Simeckova et al. (2004), Müller et al. (2009), Anttila et al. (1993)
CH$_3$C$_3$N	4.750	5/5	Moises et al. (1982), Bester et al. (1983), Bester et al. (1984)	KCl	10.270	2/2	Clouser & Gordy (1964), Caris et al. (2004)
NaCl	9.002	1/1	Clouser & Gordy (1964), Caris et al. (2002), Timp et al. (2012)	Na^{37}Cl	9.002	1/1	Same as NaCl.
AlCl	1.500	1/1	Wyse & Gordy (1972), Lide (1965), Hensel et al. (1993)	U Lines		57	

transitions that are present in the Q band range are just marginally seen.

Finally, the detection of SiC$_6$ is marginal, although possible, through several transitions from $J = 26 \rightarrow 25$ to $J = 38 \rightarrow 37$ at the 1−2 mK level (sometimes blended with lines from other species). If confirmed, this would be the first time that this Si-bearing carbon chain is seen in space.

4.5. S-bearing species

In addition to SiS (see Sect. 4.4), other detected S-bearing molecules are CS, CCS and C$_3$S. The diatomic molecule CS is detected in five isotopic substitutions, the main substitution, and ^{13}CS, C^{33}S, C^{34}S, and C^{36}S. The linear species C$_3$S has three transitions in the surveyed frequency range ($J = 6−5, 7−6,$ $8−7$), all three detected, and the $^3\Sigma$ species CCS also displays
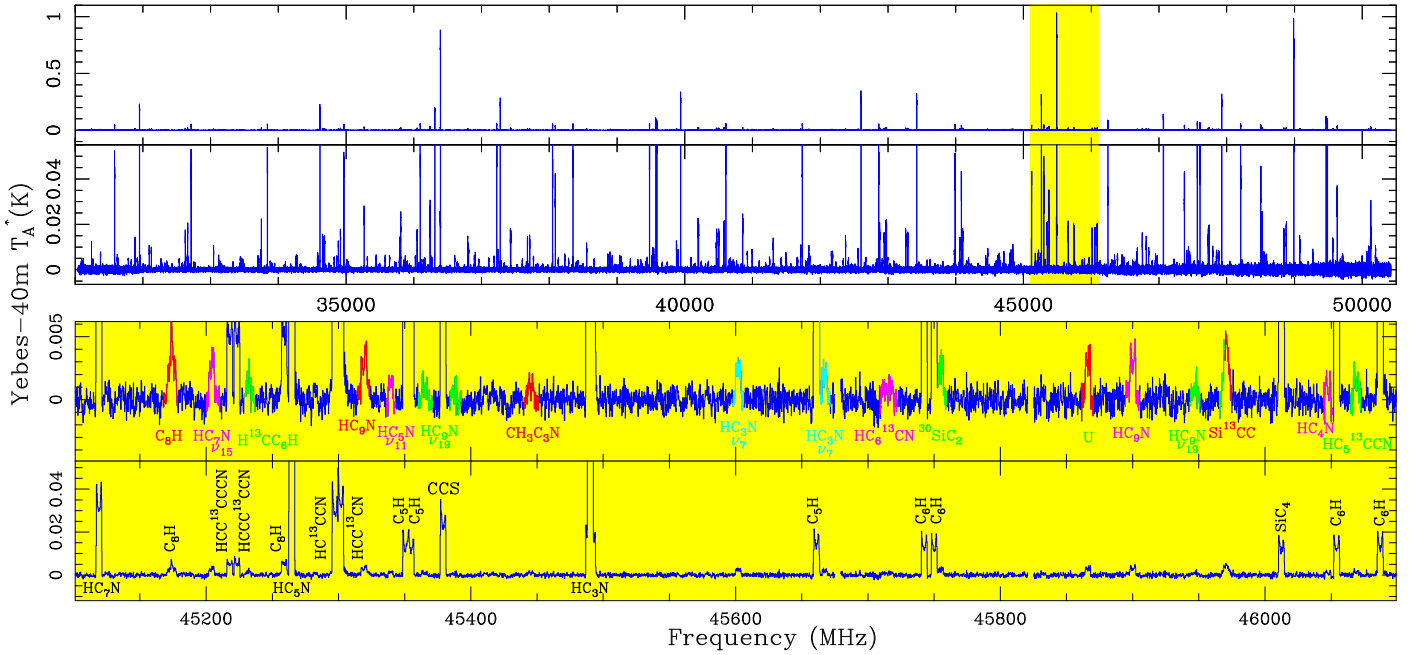
Fig. 2. Overall view of the data with a zoom around 45.6 GHz. Several weak spectral features (∼1−3 mK), revealed in this work, are shown in different colors in one of the panels.

four detected lines. The isotopic substitutions of CCS and C_3S are not seen.

4.6. Metal chlorides and cyanides

These interesting molecules in most cases appear with just one or two lines (MgCN, KCl, NaCl, $Na^{37}Cl$, and AlCl) given their molecular weight and because they are mostly diatomic or linear. NaCN, due to its bent structure, has more rotational lines, seven of them detected in this work. Two doublets were detected that correspond to the isomer MgNC. The first doublet (35 793/35 809 MHz) lies within a blended complex of lines from other molecules.

Related to the cyanides, we should mention the detection of CH_3CN (1 line), CH_3C_3N (5 lines), and the radicals MgC_3N and MgC_5N. The last two species, together with MgC_4H and MgC_6H, were discovered in space for the first time in IRC+10216 (Cernicharo et al. 2019; Pardo et al. 2021).

4.7. Cyclic molecules

In addition to SiC_2 (Sect. 4.4), the only cyclic molecule we can report as detected here is c-C_3H_2, with just two lines for both the ortho and para configuration of H spins. Only one line (the one involving the lowest energy levels within the Q band) for each species is strong and clearly detected. The other line, at 42 231.25 MHz and 42 139.19 GHz for the para and ortho species respectively, is almost ten times weaker. In addition, the 42 231.25 MHz is blended with another line from an unidentified species. For these reasons, a proper analysis using rotational diagrams needs other observed lines, for example, with the IRAM-30m telescope.

It is interesting to mention that IRC+10216 remains poor in cyclic molecules. A similar Q band survey with the same telescope on TMC-1 has discovered several cyclic molecules that are not seen in the envelope of CW Leo, such as indene and benzyne (Cernicharo et al. 2021a,b).

4.8. Latest findings

As the line identification continues and the number of unidentified features is reduced, it becomes easier to find harmonical relations in other subsets of U-lines. The great progress made in line catalogs in recent years, based on both laboratory work and ab initio calculations, is obvious. Nevertheless, spectral surveys of space objects such as this one are also part of this progress, as some species are directly discovered in them through these subsets of harmonically related U-lines. This is the case, for example, of the ν_{19} vibrational level of HC_9N, for which a series of 26 doublets, harmonically related with integer quantum numbers ranging from $J_{up} = 54$ to 80, were found among the U-lines in an early stage of analysis (Pardo et al. 2020). A fit of the observed central frequencies and line intensities allowed us to derive the rotational constants and, therefore, incorporate HC_9N ν_{19} to MADEX and the identifications in this paper.

Similarly to HC_9N ν_{19}, another harmonically related series of doublets was discovered later, resulting on the first space detection of MgC_5N. This discovery follows the previous detection by Cernicharo et al. (2019) of MgC_3N and MgC_4H, which motivated us for the search for MgC_6H in in IRC+10126. However, given the line intensities of MgC_4H, the expected lines for MgC_6H would be quite in the limit for detection. Additional observations were carried out in 2021 in order to confirm the detection of MgC_6H as finally presented in Pardo et al. (2021).

4.9. Most significant U-lines

Our work has allowed us to reduce the number of unidentified features in this work to a minimum. See Table 2.

The strongest remaining U-line at 14σ appears at a frequency of 41 711.90 MHz and was already present and not identified by Kawaguchi et al. (1995). MADEX does not provide any candidate to be the carrier, and the same applies for other catalogs.

After this strong U-line, the next unidentified line lies at 6σ at a central frequency of 42 340 MHz. This line appears as a clear and isolated spectral feature that is also present at the same
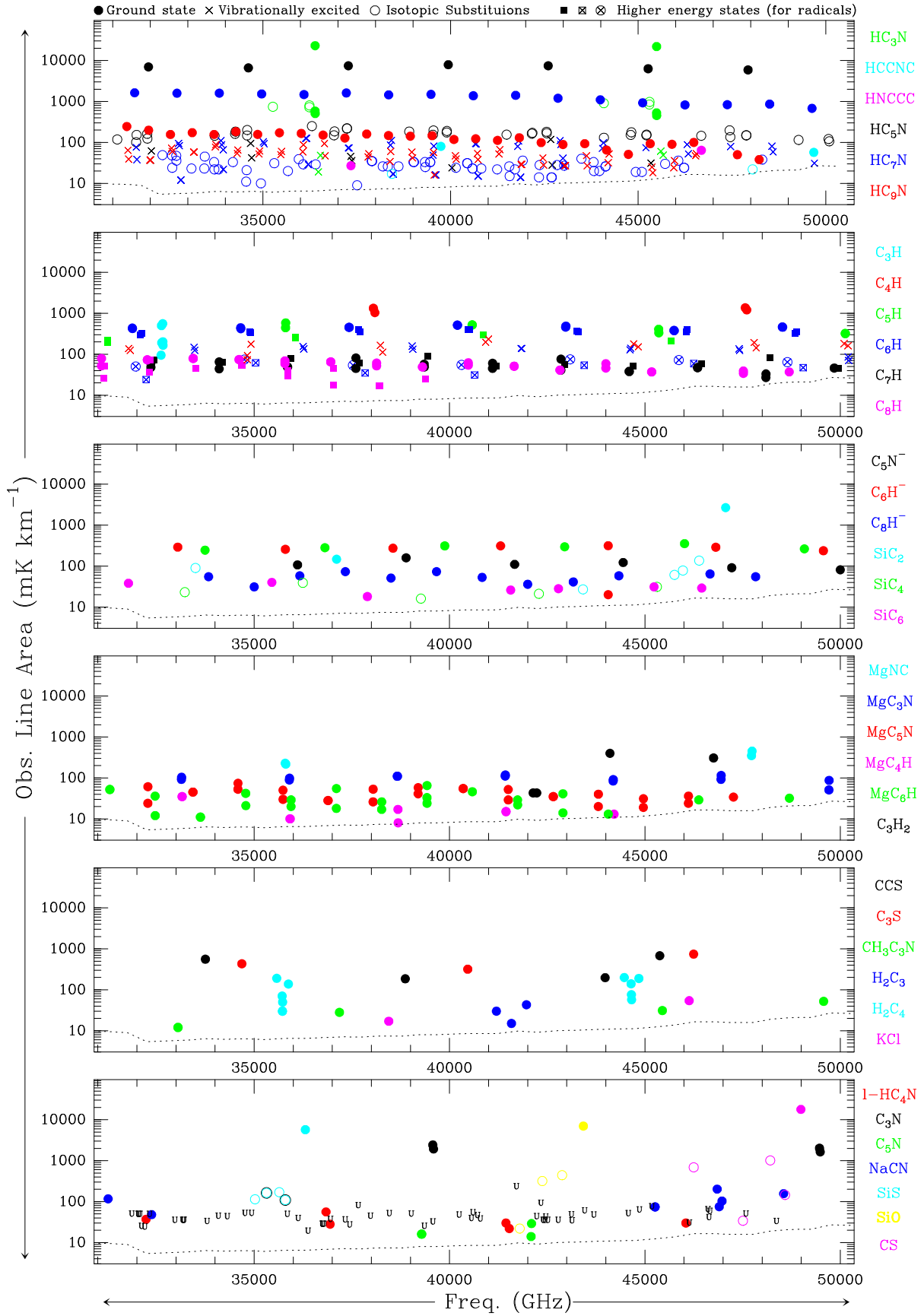
Fig. 3. Graphic summary of all lines detected in this work ($\int T_A^* dv$ vs. frequency). The dotted line marks the 1σ limit in the data according to Fig. 1. The remaining U-lines appear in the *bottom panel*.
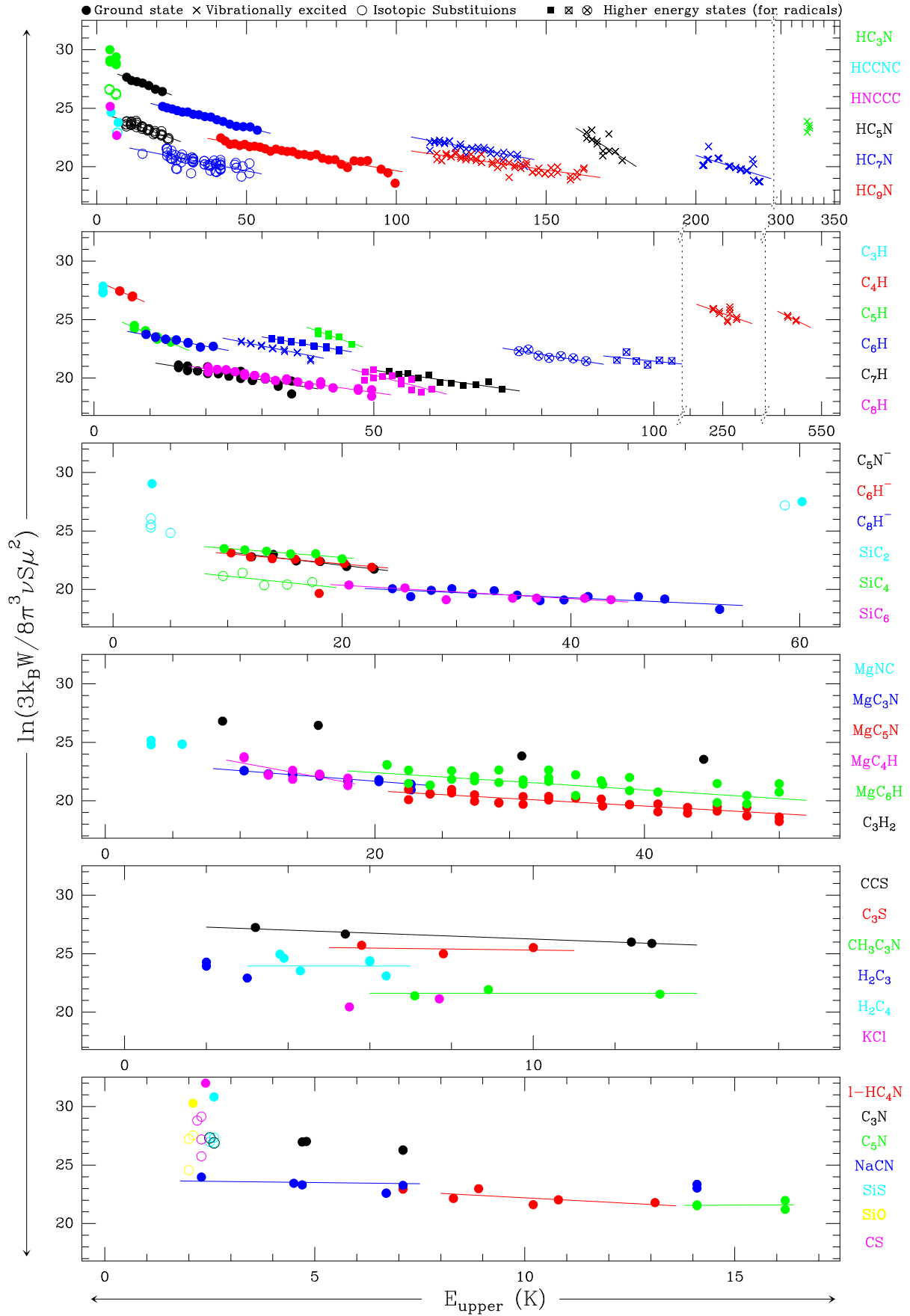
Fig. 4. More physical view of most lines detected in this work in the form of rotational diagrams. The changing telescope beam across the Q band is taken into account here through $W = \int T_{MB} dv$ in the y-axis, instead of $\int T_A^* dv$, as in Fig. 3. The values of W for each individual line can be found in Table A.1. The fits we show correspond to the molecules and results listed in Table 3.

Table 2. Observational parameters of the remaining unidentified lines.

Label	ν_{obs} (MHz)	$\int T_A^* d\nu$ (mK km s^{-1})	V_{exp} (km s^{-1})
U31869	31 868.98 (6)	50	14.6 (0.6)
U32036	32 035.92 (8)	49	13.7 (0.9)
U32040	32 039.77 (11)	49	20.1 (0.6)
U32079	32 078.51 (4)	49	12.1 (0.4)
U32119	32 118.86 (4)	25	12.2 (0.4)
U32201	32 200.71 (0)	24	11.2 (0.0)
U32322	32 322.47 (8)	49	14.5 (0.0)
U32971	32 970.52 (10)	35	13.0 (0.9)
U33174	33 174.03 (19)	35	15.6 (1.4)
U33199	33 198.51 (10)	35	16.4 (1.0)
U33202	33 201.75 (3)	35	12.9 (0.2)
U33795	33 795.37 (6)	33	14.1 (0.7)
U34083	34 083.01 (5)	44	14.0 (0.4)
U34312	34 312.00 (7)	43	14.7 (0.5)
U34766	34 766.03 (6)	52	14.4 (0.5)
U34934	34 934.28 (4)	52	15.5 (0.5)
U35849	35 848.61 (1)	49	13.6 (0.4)
U36126	36 126.03 (5)	39	14.4 (0.5)
U36380	36 380.43 (14)	19	10.5 (2.4)
U36745	36 744.91 (6)	28	10.5 (0.6)
U36750	36 749.78 (11)	28	13.8 (0.9)
U36783	36 783.37 (1)	28	14.9 (0.9)
U36952	36 951.59 (10)	37	11.8 (0.7)
U37329	37 328.60 (23)	36	14.8 (1.8)
U37443	37 442.57 (12)	27	14.1 (0.4)
U37663	37 663.08 (4)	80	14.3 (0.2)
U37977	37 977.19 (5)	44	15.0 (0.4)
U38457	38 456.75 (23)	51	14.9 (1.8)
U39021	39 020.73 (5)	50	15.2 (0.4)
U39356	39 355.87 (18)	25	14.5 (0.0)
U39575	39 574.86 (16)	32	12.4 (0.4)
U40245	40 245.20 (6)	47	14.3 (0.4)
U40560	40 559.65 (13)	39	16.7 (0.9)
U40598	40 598.39 (4)	54	15.6 (0.4)
U40714	40 714.29 (5)	46	14.5 (0.0)
U40787	40 787.22 (7)	38	14.0 (0.5)
U41712	41 711.90 (1)	233	14.6 (0.1)
U42229	42 229.33 (5)	43	13.5 (0.4)
U42340	42 340.02 (2)	92	14.1 (0.2)
U42399	42 398.99 (4)	35	14.1 (0.3)
U42443	42 443.45 (5)	35	13.9 (0.3)
U42461	42 461.14 (7)	42	14.1 (0.4)
U42514	42 513.56 (6)	35	14.1 (0.3)
U42781	42 780.72 (5)	35	14.3 (0.4)
U43118	43 118.20 (5)	48	16.0 (0.4)
U43134	43 133.53 (8)	34	12.7 (0.5)
U43457	43 457.12 (4)	60	13.6 (0.3)
U43692	43 691.87 (3)	47	13.7 (0.2)
U44574	44 574.19 (5)	51	12.4 (0.5)
U44857	44 857.46 (0)	63	14.5 (0.0)
U45176	45 175.57 (23)	75	14.5 (0.0)
U46135	46 135.23 (1)	30	11.4 (0.6)
U46613	46 613.17 (5)	64	14.6 (0.4)
U46640	46 640.00 (3)	41	14.4 (0.3)
U46662	46 661.51 (6)	58	14.5 (0.6)
U47584	47 584.28 (14)	50	11.5 (0.4)
U48365	48 364.93 (21)	33	14.5 (0.0)

position in all receiver tunings (reference central frequencies: 42 300.0, 42 280.0, and 41 370.0 MHz). A look at the MADEX catalog does not provide any plausible carrier because the only candidate, Ag^{37}Cl, does not have any emission at other frequencies in this survey, around 35 284 and 49 396 MHz, and Ag^{35}Cl is not found either.

At the 5σ level lie just two unidentified lines at the following frequencies in rounded numbers: 35 849 and 37 663 MHz. These two lines again appear isolated and well detected in all three different receiver tunings at the same position. Again, no answers are found in MADEX about possible carriers. It is worth noting, in any case, that we are talking about features with peak intensities below 3 mK in the T_A^* scale.

At the 4σ level we have only one unidentified line, at 43 457.12 MHz. Again, it appears at the same position in all three receiver tunings, but no carrier has been found for it yet.

4.10. Unidentified lines at the 3σ level

In addition to the most significant unidentified lines we discussed in Sect. 4.9, 52 more features remain unidentified just at the 3σ level and with line widths within ±20% from that typical of the source. Most of these features are in fact at ~1 mK level so that some of them could just be artifacts that would disappear on deeper integrations (which we plan to do) or might be baseline effects, although we do not have evidence to remove any of the remaining features, as we have done with several other in our data reduction process. Table 2 should therefore be kept as a reference for follow-up in future works.

5. Procedure for line identification

The first thing to say in this section is that not all the identifications are 100% certain, although we are quite confident about most of them. The main doubts arise when (i) the frequency coincidence is typically not within ~1 MHz, (ii) the line width is too narrow or too broad with respect to the typical line width of the source, (iii) there is a close blending with a stronger line, and (iv) only one line for a given species is found and we cannot confirm it from other lines detected at higher frequencies with other telescopes. These circumstances are pointed out in our line identification Table A.1 when necessary.

The exhaustive information of our IRC+10216 *Q* band survey with the Yebes-40m telescope is provided in two forms, the detailed Figs. A.1–A.39 and, also, Table A.1, available at the CDS.

For our data analysis and line identification process, we have defined a reference file containing the data smoothed to a resolution of 229 kHz (six-channel smoothing from the original output), from which we have removed all artifacts (spikes and baseline undulations) as best we could. Then we fit all the spectral features in the data using the method SHELL implemented in the GILDAS package, which is adequate for the CW Leo expanding envelope. We left the expansion velocity as a free parameter in this fit as an additional check for the line identification process (see below). The fitted line profiles were stored as a third column in the reference file so that we can incorporate them to the figures for convenience. We created a separate file containing the MADEX catalog entries that we identified as corresponding to the observed spectral features, and another file storing the SHELL method fitting parameters. The first file (irc10216_qband.dat) was used to

Table 3. Results from rotational diagram fits in this work.

Molecule	# lines	$T_{\rm rot}$ (K)	$N_{\rm col}$ (cm^{-2})	$Z_{\rm rot}$	Comments
HC$_5$N	7	10.1 ± 0.6	$(4.2 \pm 0.4) \times 10^{14}$	158.80	Reliable fit
HC$_5$N $v_{11} = 1$	12	6.2 ± 1.8	$(7 \pm 5) \times 10^{12}$	195.20	Large data dispersion
H^{13}CCCCCN	8	10.0 ± 1.7	$(9.7 \pm 2.7) \times 10^{12}$	161.52	Reliable fit
HC^{13}CCCCN	8	14.4 ± 2.6	$(8.2 \pm 1.7) \times 10^{12}$	228.04	Reliable fit
HCC^{13}CCCN	7	10.4 ± 1.3	$(1.00 \pm 0.19) \times 10^{13}$	162.42	Reliable fit
HCCC^{13}CCN	7	10.6 ± 1.7	$(1.00 \pm 0.25) \times 10^{13}$	166.20	Reliable fit
HCCCC^{13}CN	8	9.2 ± 0.6	$(1.09 \pm 0.13) \times 10^{13}$	145.42	Reliable fit
HC$_7$N	17	15.8 ± 0.4	$(1.95 \pm 0.11) \times 10^{14}$	583.44	Reliable fit
HC$_7$N $v_{15} = 1$	31	21.3 ± 1.7	$(2.0 \pm 0.3) \times 10^{13}$	1572.97	Reliable fit (3 points removed)
HC$_7$N $v_{15} = 2$	26	12.6 ± 2.5	$(1.0 \pm 0.5) \times 10^{13}$	1358.51	Large data dispersion
H^{13}CCCCCCCN	11	23 ± 4	$(3.0 \pm 0.8) \times 10^{12}$	879.75	Reliable fit (1 point removed)
HC^{13}CCCCCCN	8	15 ± 7	$(3.31 \pm 3.41) \times 10^{12}$	559.13	Large data dispersion
HCC^{13}CCCCCN	10	19 ± 6	$(3.5 \pm 2.1) \times 10^{12}$	713.79	Large data dispersion
HCCC^{13}CCCCN	10	23 ± 4	$(2.7 \pm 0.8) \times 10^{12}$	836.22	Reliable fit (2 points removed)
HCCCC^{13}CCCN	6	16 ± 3	$(3.9 \pm 1.7) \times 10^{12}$	573.14	Reliable fit
HCCCCC^{13}CCN	11	22 ± 6	$(2.7 \pm 1.3) \times 10^{12}$	824.82	Large data dispersion
HCCCCCC^{13}CN	9	31 ± 10	$(3.2 \pm 1.1) \times 10^{12}$	1156.63	Reliable fit (1 point removed)
HC$_9$N	30	22.9 ± 1.1	$(4.5 \pm 0.6) \times 10^{13}$	1644.03	Reliable fit (1 point removed)
HC$_9$N $v_{19} = 1$	50	28.0 ± 2.2	$(2.4 \pm 0.4) \times 10^{13}$	4009.46	Reliable fit (1 point removed)
l-HC$_4$N	6	5.1 ± 2.5	$(3.9 \pm 3.7) \times 10^{12}$	126.85	Large data dispersion
C$_4$H	4	4.9 ± 0.6	$(1.84 \pm 0.25) \times 10^{14}$	86.42	Reliable fit
C$_4$H $v_7 = 1$	10	10 ± 5	$(6.6 \pm 2.0) \times 10^{13}$	314.65	Large data dispersion
C$_4$H $v_7 = 2$	4	6.4 ± 1.3	$(2.2 \pm 0.4) \times 10^{13}$	113.77	Reliable fit
C$_5$H $^2\Pi_{1/2}$	8	5.0 ± 0.4	$(2.7 \pm 0.5) \times 10^{13}$	172.74	Reliable fit
C$_5$H $^2\Pi_{3/2}$	8	5.9 ± 0.8	$(2.52 \pm 2.48) \times 10^{14}$	10.67	Moderate data dispersion
C$_6$H $^2\Pi_{3/2}$	14	11.0 ± 0.8	$(1.51 \pm 0.14) \times 10^{13}$	334.91	Reliable fit
C$_6$H $^2\Pi_{1/2}$	14	12.4 ± 0.6	$(1.23 \pm 0.18) \times 10^{13}$	66.83	Reliable fit
C$_6$H $v_{11} = 1$	14	10.4 ± 0.5	$(9.3 \pm 0.7) \times 10^{12}$	310.61	Reliable fit (2 points removed)
C$_6$H $^2\Delta_{5/2}$ $v_{11} = 1$	6	13 ± 3	$(2.0 \pm 0.5) \times 10^{12}$	201.51	Moderate data dispersion
C$_6$H $^2\Delta_{3/2}$ $v_{11} = 1$	7	21 ± 13	$(1.4 \pm 0.7) \times 10^{12}$	311.75	Large data dispersion
C$_7$H $^2\Pi_{1/2}$	22	13.2 ± 1.4	$(5.1 \pm 1.0) \times 10^{12}$	1260.39	Reliable fit (1 point removed)
C$_7$H $^2\Pi_{3/2}$	11	14.7 ± 2.2	$(3.2 \pm 2.0) \times 10^{12}$	110.99	Moderate data dispersion
C$_8$H $^2\Pi_{3/2}$	30	14.8 ± 0.6	$(8.9 \pm 0.9) \times 10^{12}$	2111.08	Reliable fit (1 point removed)
C$_8$H $^2\Pi_{1/2}$	16	8.0 ± 1.4	$(1.15 \pm 1.38) \times 10^{13}$	35.16	Large data dispersion
C$_5$N$^-$	6	8.8 ± 1.4	$(4.9 \pm 1.6) \times 10^{12}$	132.62	Reliable fit
C$_6$H$^-$	7	11.4 ± 1.0	$(4.3 \pm 0.6) \times 10^{12}$	173.51	Reliable fit
C$_8$H$^-$	13	23 ± 5	$(1.1 \pm 0.4) \times 10^{12}$	810.24	Reasonable fit. Large data dispersion
SiC$_4$	6	12.9 ± 1.8	$(6.2 \pm 1.0) \times 10^{12}$	175.36	Reliable fit
^{29}SiC$_4$	5	10 ± 6	$(5.73 \pm 5.06) \times 10^{11}$	134.88	Large data dispersion
SiC$_6$	7	17.3 ± 2.5	$(1.3 \pm 0.4) \times 10^{12}$	588.57	Reliable fit (1 point removed)
CCS	4	7.9 ± 1.1	$(4.0 \pm 0.7) \times 10^{13}$	44.48	Reliable fit
C$_3$S	3	23.60 ± 96.85	$(2.58 \pm 3.60) \times 10^{13}$	170.50	Very high data dispersion
NaCN	7	24 ± 13	$(8.5 \pm 1.7) \times 10^{12}$	425.76	Large data dispersion (1 point removed)
MgC$_3$N	14	11.1 ± 0.9	$(5.2 \pm 0.6) \times 10^{12}$	336.00	Reliable fit (1 point removed)
MgC$_5$N	30	15.4 ± 1.8	$(4.7 \pm 1.3) \times 10^{12}$	1109.27	Reliable fit (1 point removed)
MgC$_4$H	10	4.7 ± 1.2	$(1.5 \pm 1.3) \times 10^{13}$	140.43	Large data dispersion
MgC$_6$H	30	24.8 ± 8.9	$(2.0 \pm 0.9) \times 10^{13}$	966.24	Large data dispersion

Notes. $T_{\rm rot}$: Rotational temperature. $N_{\rm col}$: Column density. $Z_{\rm rot}$: Partition function. The resulting fits are plotted in Fig. 4 on top of the data points we used for the fits (extracted from the individual line fits as listed in Table A.1). Species with unreliable fits due to a very low number of data points or extremely high data dispersion in them, are not shown. These species, and others with a very low number of detected lines here, will be revisited in future publications of similar 4.3 to 1.0 mm surveys carried out with the IRAM-30m telescope.

create figures. The other two files (irc10216_qband.lines and irc10216_qband.parameters) were used as inputs for a fortran script that was especially designed for this paper. It automatically created Tables 1 and A.1, calculating in particular $W = \int T_{\rm MB} dv$, where the changing telescope beam across the Q band is taken into account. It also updated the numbers and percentages of identified lines given in the Abstract and in the main text. This allowed us to introduce criteria in our analysis and new fits

or baseline corrections that were immediately checked throughout all the data in a consistent way. The results were updated in our manuscript without the need to repeatedly confirm them by hand. This also provides a systematic way of reconfirming the whole work if, for example, more observations are added and, therefore, the noise level is improved and/or more frequencies are added.

The most significant line parameters (theoretical + observed) of all spectral lines that can be assigned to an identified molecular species are given in Table A.1. The accumulated number of distinguishable lines for each species is provided in the last column of that table, which is the basis for building Figs. 3 and 4. The observed values listed in Table A.1, including errors in parentheses affecting the last digits of the observed frequency and the expansion velocity, come from the line fits performed over the data with the Gildas SHELL method, as shown in Figs. A.1–A.39. An error of 0 or 0.0 means the given observed frequency (ν_{obs}) and/or expansion velocity (V_{exp}) has been forced in the fit. The figures themselves have labels to identify the positions of all the lines that appear in Table A.1, and they also label the U-lines listed in Table 2. The frequency scale in all tables and figures assumes a velocity of the source with respect to the local standard of rest of $-26.5\,\mathrm{km\,s^{-1}}$. The changing telescope beam across the *Q* band is taken into account in the calculation of $W = \int T_{MB}\mathrm{d}v$.

6. Legacy and summary

The main purpose of this work was to provide a reference in the *Q* band for further investigations of the molecular content of the circumstellar envelope of CW Leo using other bands. For this reason we provide the full data set and line fits as online material for the scientific community.

The results published here, first of all, due to the large number of lines and molecules that were detected, provide an opportunity to give a very good diagnostics for the rotational temperature. To do this, we used the molecules in Table 3 with reliable fits. We provide three results. The first two are weighted averages using the number of detected lines and the derived column density. The third value is just an arithmetic average. The values are: 16.9, 11.4, and 14.1 K, respectively.

The only isotopic ratio we can give in this work is ^{12}C/^{13}C using HC$_5$N because the lines from the HC$_7$N isotopologs are weak and only two lines from HC$_3$N and its isotopologs are available. The result (^{12}C/^{13}C = 43.0 ± 4.7) agrees well with previous works, 44 ± 3 from Kahane et al. (1992) and 45 ± 3 from Cernicharo et al. (2000).

The other important contribution of this work is that it provides a large amount of data for molecular column densities to be used for comparisons with results from chemical models of this source, together with the full 4.3−1.0 mm data from the IRAM-30m telescope, which should also be published soon. Detected molecules with very few lines in the *Q* band are left for analysis in this future publication, for which the data from them published here (Table A.1 and Figs. A.1–A.39) are to be combined with those obtained with the IRAM-30m telescope.

We have presented the full results of *Q* band (31.0−50.3 GHz) deep integration toward IRC+10216, one of the richest and more exhaustively studied molecular stellar envelopes in the sky. This work represents a great improvement over previously available surveys in the same frequency range in terms of noise level and line identification because we used the most recent line catalogs. Prior to this publication, a series of papers has presented the identification from these data of

new molecular species and/or vibrational states that were never before detected in space of known molecular species. The list of U-lines is almost entirely reduced to features at $3-4\sigma$ level, with the exception of three lines that still defy identification.

In order to provide a useful legacy from this project, we have proceeded to fit all the spectroscopic features in the data to provide detailed figures of data versus fit, tables with line identifications with theoretical versus experimental line parameters, and, finally, rotational diagrams to explore the physical conditions of IRC+10216 through the molecular species present in this work.

References

Alexander, A. J., Kroto, H. W., & Walton, D. R. M. 1976, J. Mol. Spectr., 62, 175
Allen, M. D., Evenson, K. M., Brown, J. M., et al. 2001, J. Mol. Spectr., 209, 143
Anderson, M. A., Steimle, T. C., & Ziurys, L. M. 1994, ApJ, 429, L41
Anttila, R., Horneman, V. M., Koivusaari, M., et al. 1993, J. Mol. Spectr., 157, 198
Aoki, K., & Ikuta, S. 1993, J. Chem. Phys., 99, 3809
Bester, M., Tanimoto, M., Vowinkel, B., et al. 1983, Z. Naturforschung, 38, 64
Bester, M., Yamada, K., Winnewisser, G., et al. 1984, A&A, 137, L20
Bizzocchi, L., Degli Esposti, C., & Botschwina, P. 2004, J. Mol. Spectr., 225, 145
Blanksby, S. J., McAnoy, A. M., Dua, S., et al. 2001, MNRAS, 328, 89
Bogey, M., Demuynck, C., & Destombes, J. L. 1986, Chem. Phys. Lett., 125, 383
Botschwina, P. 1996, Chem. Phys. Lett., 259, 627
Botschwina, P., Horn, M., Seeger, S., et al. 1992, Chem. Phys. Lett., 195, 427
Botschwina, P., Horn, M., Markey, K., et al. 1997, Mol. Phys., 92, 381
Caris, M., Lewen, F., & Winnewisser, G. 2002, Z. Naturforschung, 57, 663
Caris, M., Lewen, F., Muller, H. S. P., & Winnewisser, G. 2004, J. Mol. Struct., 695, 243
Cazzoli, G., & Puzzarini, C. 2006, J. Mol. Spectr., 240, 153
Cernicharo, J. 1985, Internal IRAM Report (Granada: IRAM)
Cernicharo, J. 2012, ECLA 2011: Proc. of the European Conference on Laboratory Astrophysics, eds. C. Stehl, C. Joblin, & L. d'Hendecourt (Cambridge: Cambridge University Press), EAS Publ. Ser., 251
Cernicharo, J., Guélin, M., Kahane, K., et al. 1991, A&A, 246, 213
Cernicharo, J., Guélin, M., & Kahane, C. 2000, A&AS, 142, 181
Cernicharo, J., Guélin, M., Agúndez, M., et al. 2008, ApJ, 688, L83
Cernicharo, J., Agúndez, M., Kahane, C., et al. 2011, A&A, 529, L3
Cernicharo, J., Marcelino, N., Agúndez, M., et al. 2015, A&A, 575, A91
Cernicharo, J., Cabezas, C., Pardo, J. R., et al. 2019, A&A, 63, L2
Cernicharo, J., Agúndez, M., Cabezas, C., et al. 2021a, A&A, 649, L15
Cernicharo, J., Agúndez, M., Kaiser, R. I., et al. 2021b, A&A, 652, L9
Chen, W., Novick, S. E., McCarthy, M. C., Gottlieb, C. A., & Thaddeus, P. 1995, J. Chem. Phys., 103, 7828
Cho, S.-H., & Saito, S. 1998, ApJ, 496, L51
Clouser, P. L., & Gordy, W. 1964, Phys. Rev., 134, A863
Creswell, R. A., Winnewisser, G., & Gerry, M. C. L. 1977, J. Mol. Spectr., 65, 420
Degli Esposti, C., & Bizzocchi, L. 2004, ApJ, 614, 518
Ebenstein, W. L., & Muenter, J. S. 1984, J. Chem. Phys., 80, 3989
Gordon, V. D., Nathan, E. S., Apponi, A. J., et al. 2000, J. Chem. Phys., 113, 5311
Gottlieb, C. A., Gottlieb, E. W., Thaddeus, P., & Kawamura, H. 1983, ApJ, 275, 916
Gottlieb, C. A., Vrtilek, J. M., Gottlieb, E. W., Thaddeus, P., & Hjalmarson, A. 1985, ApJ, 294, L55
Gottlieb, C. A., Vrtilek, J. M., & Thaddeus, P. 1989, ApJ, 343, L29
Gottlieb, C., Myers, P. C., & Thaddeus, P. 2003, ApJ, 588, 655
Gripp, J., Guarnieri, A., Stahl, W., et al. 2000, J. Mol. Struct., 526, 81
Groenewegen, M. A. T., Barlow, M. J., Blommaert, J. A. D. L., et al. 2012, A&A, 543, L8
Guarnieri, A., Hinze, R., Krüger, M., et al. 1992, J. Mol. Spectr., 156, 39

Guélin, M., Friberg, P., & Mezaoui, A. 1982, A&A, 109, 23
Guélin, M., Patel, N. A., Bremer, M., et al. 2018, A&A, 610, A4
Gupta, H., Brünken, S., Tamassia, F., et al. 2007, ApJ, 655, L57
Halfen, D. T., & Ziurys, L. M. 2011, ApJ, 730, 107
Hensel, K. D., Styger, C., Jäger, W., et al. 1993, J. Chem. Phys., 99, 3320
Hirahara, Y., Ohshima, Y., & Endo, Y. 1993, ApJ, 403, L83
Hirano, T., Ishii, K., Odaka, T. E., et al. 2002, J. Mol. Spectr., 215, 42
Ikuta, S., Tsuboi, T., & Aoki, K. 2000, J. Mol. Struct., 528, 297
Kahane, C., Cernicharo, J., Gómez-González, J., & Guélin, M. 1992, A&A, 256, 235
Kaifu, N., Ohishi, M., Kawaguchi, K., et al. 2004, PASJ, 56, 69
Kanata, H., Yamamoto, S., & Saito, S. 1987, Chem. Phys. Lett., 140, 221
Kasai, Y., Sumiyoshi, Y., & Endo, Y. 1997, ApJ, 477, L65
Kawaguchi, K., Takano, S., Ohishi, M., et al. 1992, ApJ, 396, L49
Kawaguchi, K., Kagi, E., Hirano, T., et al. 1993, ApJ, 406, L39
Kawaguchi, K., Kasai, Y., Ishikawa, S., & Kaifu, N. 1995, PASJ, 47, 853
Killian, T. C., Vrtilek, T. C., & Gottlieb, J. M. 1990, ApJ, 365, L89
Kokkin, D. L., Brünken, S., Young, K. H., et al. 2011, ApJS, 196, 17
Lee, S. 1997, Chem. Phys. Lett., 268, 69
Lide, D. R. 1965, J. Chem. Phys., 42, 1013
Linnartz, H., Motylewski, T., Vaizert, O., et al. 1999, J. Mol. Spectr., 197, 1
Lovas, F. J., Suenram, R. D., Ogata, T., & Yamamoto, S. 1992, ApJ, 399, 325
Mallinson, P. D., & de Zafra, R. L. 1978, Mol. Phys., 36, 827
Manson, E. L., Jr., Clark, W. W., DeLucia, F. C., & Gordy, W. 1977, Phys. Rev. A, 15, 223
Mbosei, L., Fayt, A., Dréan, P., & Cosléou, J. 2000, J. Mol. Struct., 517, 271
McCarthy, M. C., Gottlieb, C. A., Thaddeus, P., Horn, M., & Botschwina, P. 1995, J. Chem. Phys., 103, 7820
McCarthy, M. C., Travers, M. J., Kovács, A., Gottlieb, C. A., & Thaddeus, P. 1996, A&A, 309, L31
McCarthy, M. C., Travers, M. J., Kovács, A., Gottlieb, C. A., & Thaddeus, P. 1997, ApJ, 113, 105
McCarthy, M. C., Chen, W., Apponi, A. J., Gottlieb, C. A., & Thaddeus, P. 1999, ApJ, 520, 158
McCarthy, M. C., Levine, E. S., Apponi, A. J., & Thaddeus, P. 2000, J. Mol. Spectr., 203, 75
McCarthy, M. C., Fuchs, G. W., Kucera, J., Winnewisser, G., & Thaddeus, P. 2003, J. Chem. Phys., 118, 3549
McCarthy, M. C., Gottlieb, C. A., Gupta, H., & Thaddeus, P. 2006, ApJ, 652, L141
Moises, A., Boucher, D., Burie, J., et al. 1982, J. Mol. Spectr., 92, 497
Mollaaghababa, R., Gottlieb, C. A., Vrtilek, J. M., & Thaddeus, P. 1991, ApJ, 368, L19

Müller, H. S. P., McCarthy, M. C., Bizzocchi, L., et al. 2007, Phys. Chem. Chem. Phys., 9, 1579
Müller, H. S. P., Drouin, B. J., & Pearson, J. C. 2009, A&A, 506, 1487
Ohishi, M., Kaifu, N., Kawaguchi, K., et al. 1989, ApJ, 345, L83
Ohshima, Y., & Endo, Y. 1992, J. Mol. Spectr., 153, 627
Oswald, M., & Botschwina, P. 1995, J. Mol. Spectr., 169, 181
Oyama, T., Ozaki, H., Sumiyoshi, Y., et al. 2020, ApJ, 890, 39
Pardo, J. R., Cernicharo, J., & Serabyn, E. 2001, IEEE Trans. Antennas Propag., 49, 12
Pardo, J. R., Bermúdez, C., Cabezas, C., et al. 2020, A&A, 640, L13
Pardo, J. R., Cabezas, C., Fonfría, J. P., et al. 2021, A&A, 652, L13
Pavone, F. S., Zink, L. R., Prevedelli, M., et al. 1990, J. Mol. Spectr., 144, 45
Raymonda, J. W., Muenter, J. S., & Kemplerer, W. A. 1970, J. Chem. Phys., 52, 3458
Saito, S., Kawaguchi, K., Yamamoto, S., et al. 1987, ApJ, 317, L115
Sanz, M. E., McCarthy, M. C., & Thaddeus, P. 2003, J. Chem. Phys., 119, 11715
Simeckova, M., Urban, S., Fuchs, U., et al. 2004, J. Mol. Spectr., 226, 123
Spezzano, S., Tamassia, F., Thorwirth, S., et al. 2012, ApJS, 200, 1
Steimle, T. C., & Bousquet, R. R. 2001, J. Chem. Phys., 115, 5203
Suenram, R. D., & Lovas, F. J. 1994, ApJ, 429, L89
Suenram, R. D., Lovas, F. J., & Matsumura, K. 1989, ApJ, 342, L103
Tang, J. A., & Saito, S. 1995, J. Mol. Spectr., 169, 92
Tang, J. A., Sumiyoshi, Y., & Endo, Y. 1999, Chem. Phys. Lett., 315, 69
Tercero, F., López-Pérez, J. A., Gallego, J. D., et al. 2021, A&A, 645, A37
Thaddeus, P., Vrtilek, J. M., & Gottlieb, C. A. 1985, ApJ, 299, L63
Thaddeus, P., Gottlieb, C. A., Gupta, H., et al. 2008, ApJ, 677, 1139
Thorwirth, S., Müller, H. S. P., & Winnewisser, G. 2000, J. Mol. Spectr., 204, 133
Thorwirth, S., Müller, H. S. P., & Winnewisser, G. 2001, Phys. Chem. Chem. Phys., 3, 1236
Tiemann, E., Renwanz, E., Hoeft, J., et al. 1972, Z. Naturforschung, 27, 1566
Timp, B. A., Doran, J. L., Iyer, S., et al. 2012, J. Mol. Spectr., 271, 20
Van Vaals, J. J., Meerts, W. L., & Dymanus, A. 1984, Chem. Phys., 86, 147
Vrtilek, J. M., Gottlieb, C. A., & Thaddeus, P. 1987, ApJ, 314, 716
Vrtilek, J. M., Gottlieb, C. A., Gottlieb, E. W., Killian, T. C., & Thaddeus, P. 1990, ApJ, 364, L53
Winnewisser, G., & Cook, R. L. 1968, J. Mol. Spectr., 28, 266
Woon, D. E. 1995, Chem. Phys. Lett., 244, 45
Wyse, F. C., & Gordy, W. 1972, J. Chem. Phys., 56, 2130
Yamamoto, S., Saito, S., Kawaguchi, K., et al. 1987, ApJ, 317, L119
Yamamoto, S., Saito, S., Suzuki, H., et al. 1990a, ApJ, 348, 363
Yamamoto, S., Saito, S., & Kawaguchi, K. 1990b, ApJ, 361, 318
Zelinger, Z., Amano, T., Ahrens, V., et al. 2003, J. Mol. Spectr., 220, 233

Appendix A: Additional figures
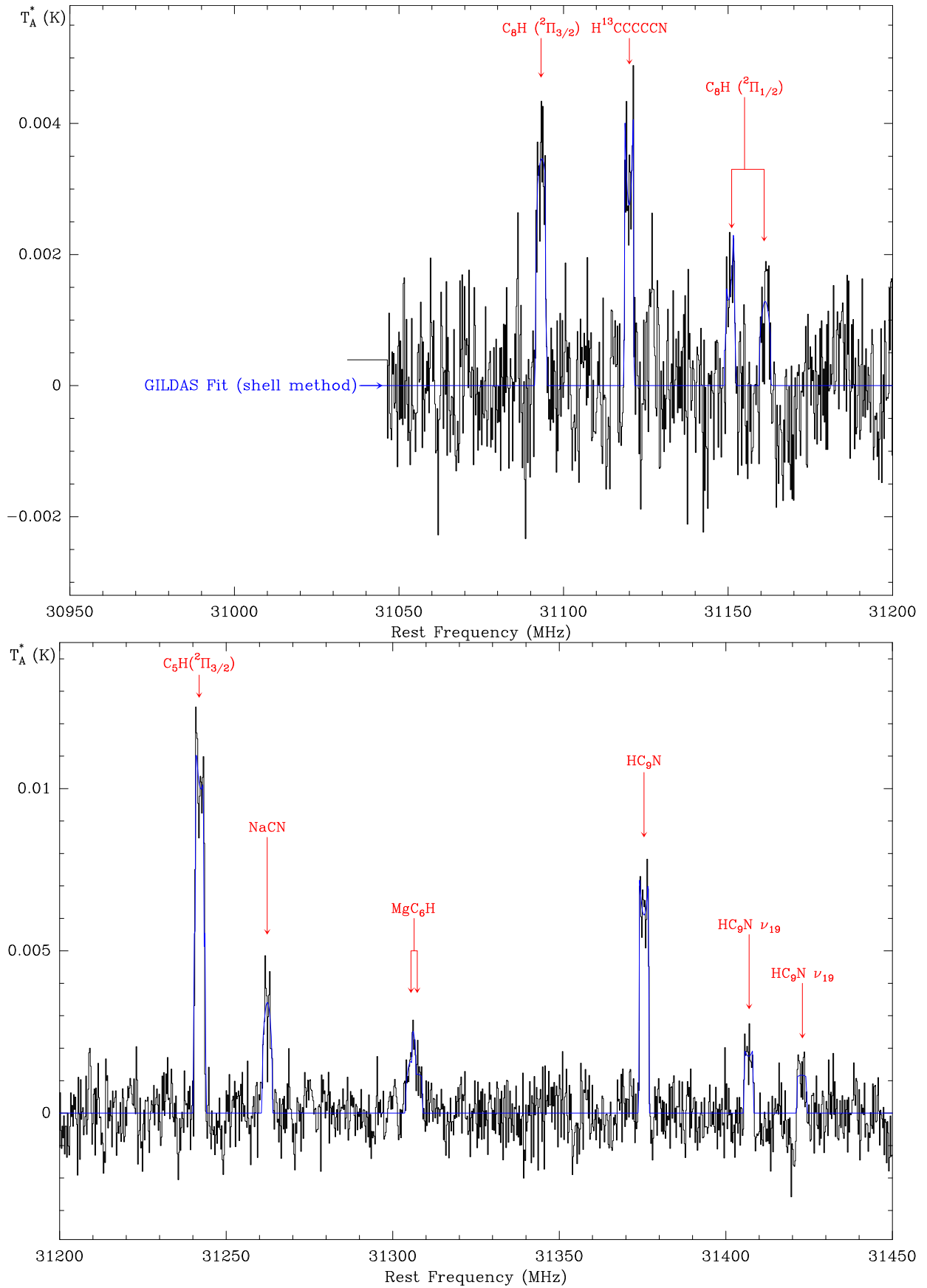
Fig. A.1. IRC+10216 Yebes-40m data, line fits, and labels from 30950 to 31450 GHz.
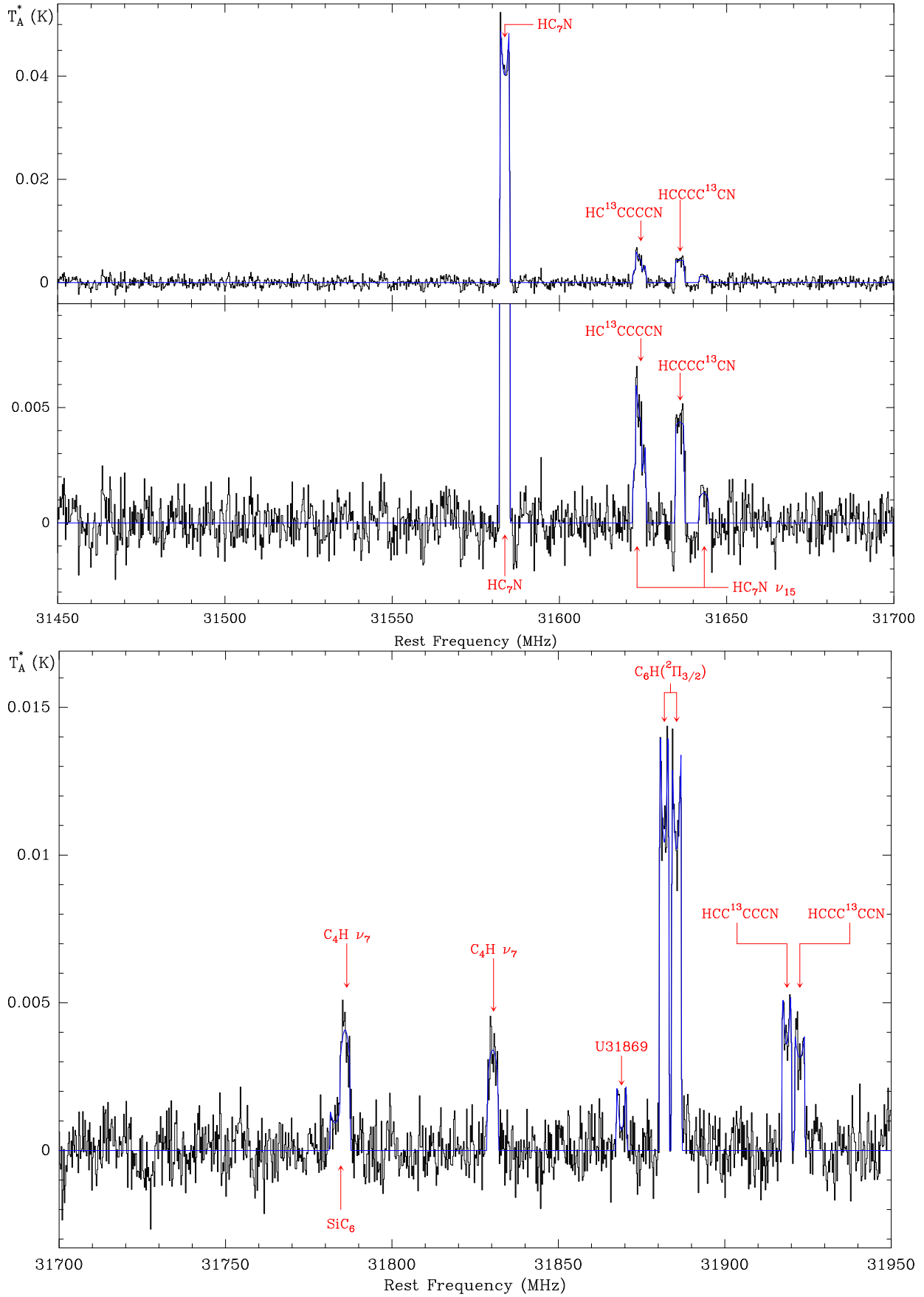
Fig. A.2. IRC+10216 Yebes-40m data, line fits, and labels from 31450 to 31950 GHz.
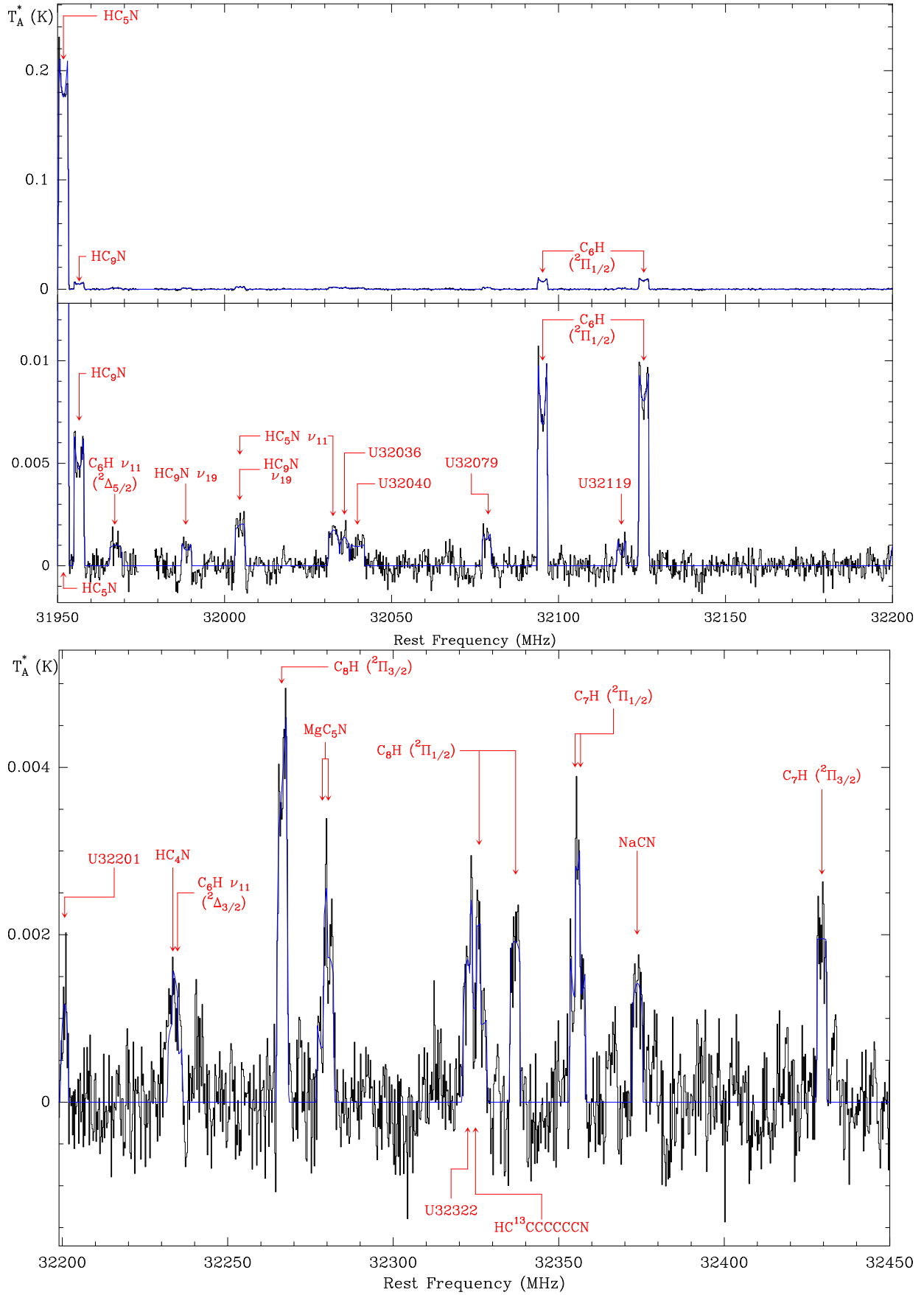
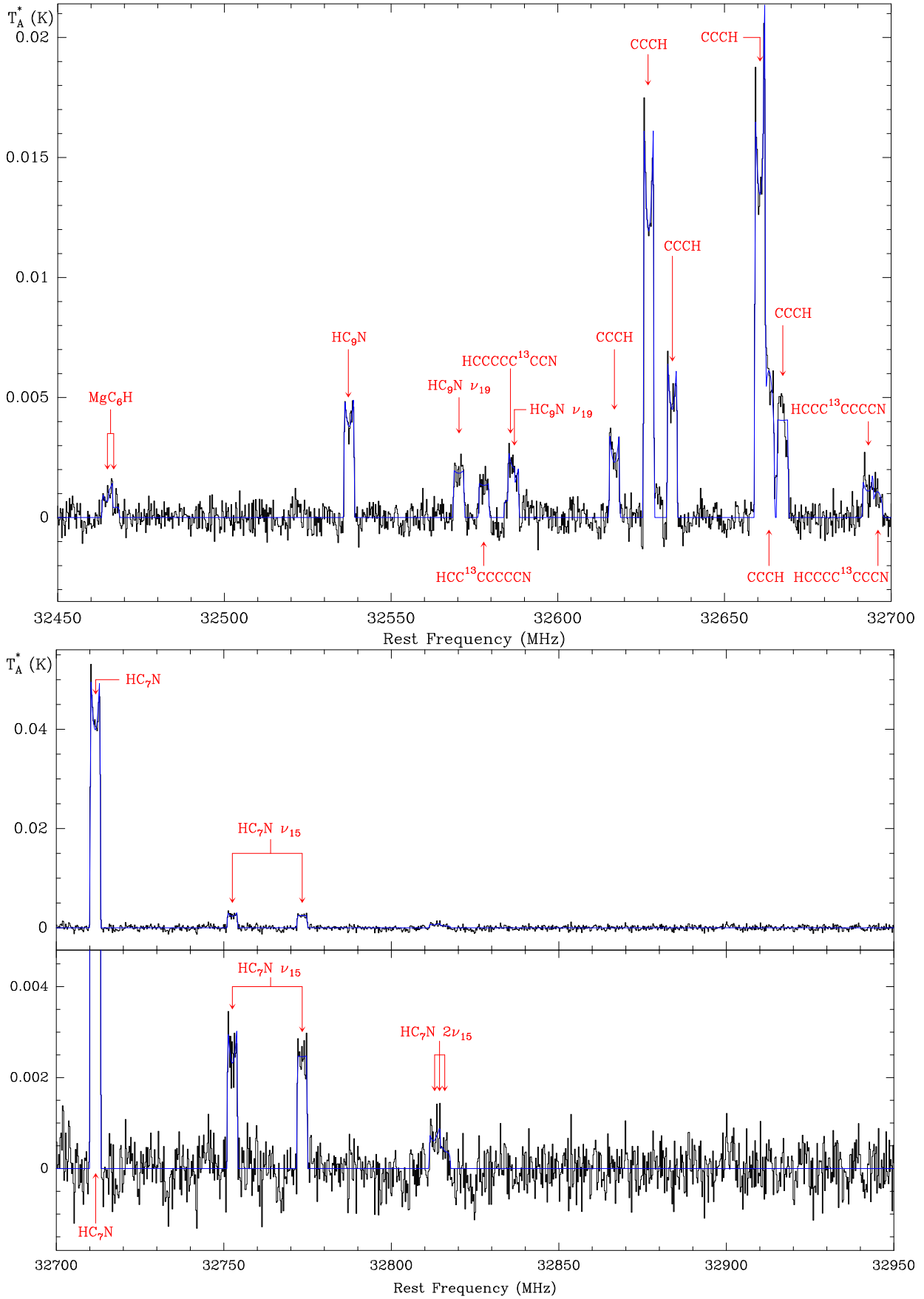**Fig. A.3.** IRC+10216 Yebes-40m data, line fits, and labels from 31950 to 32450 GHz.

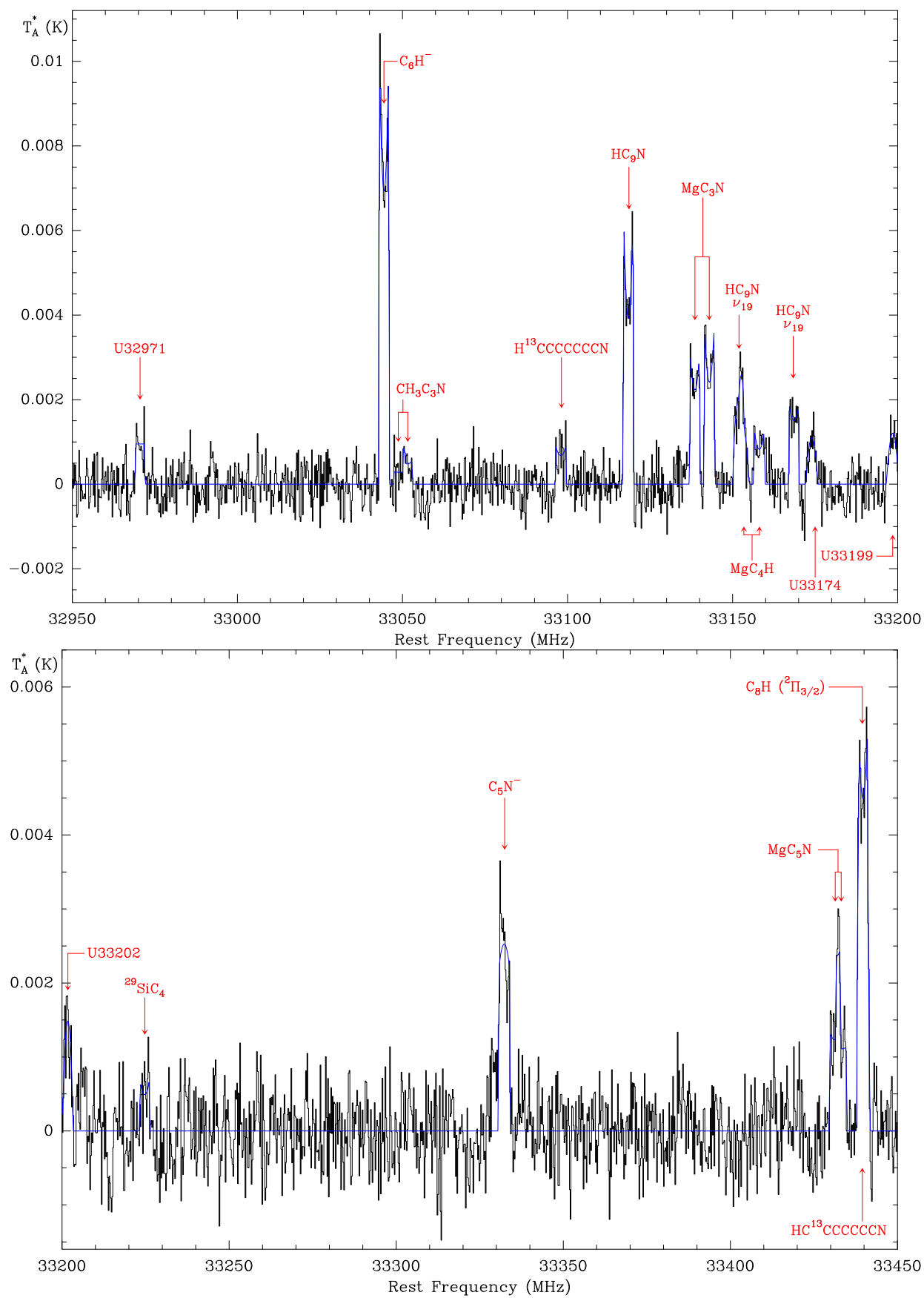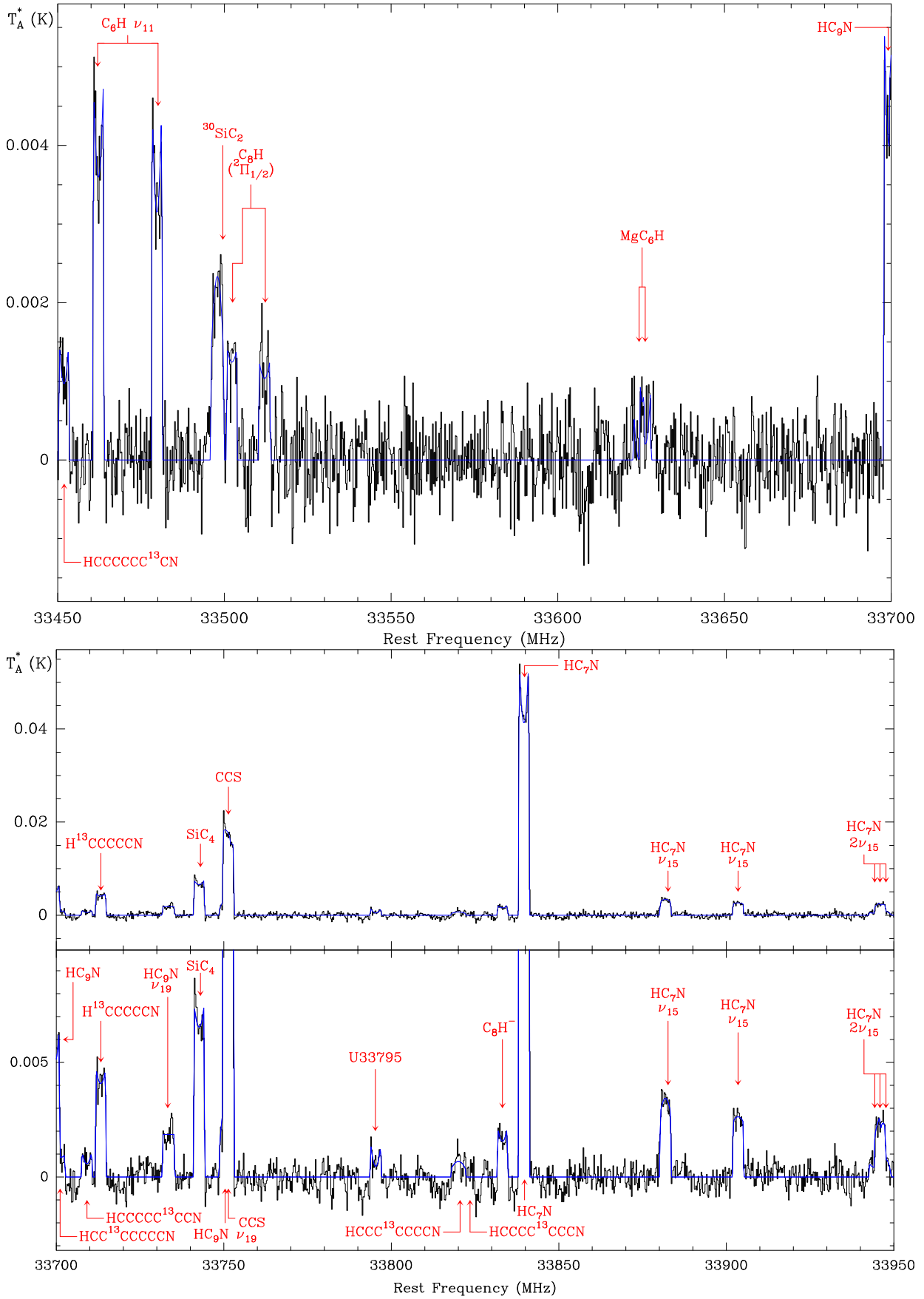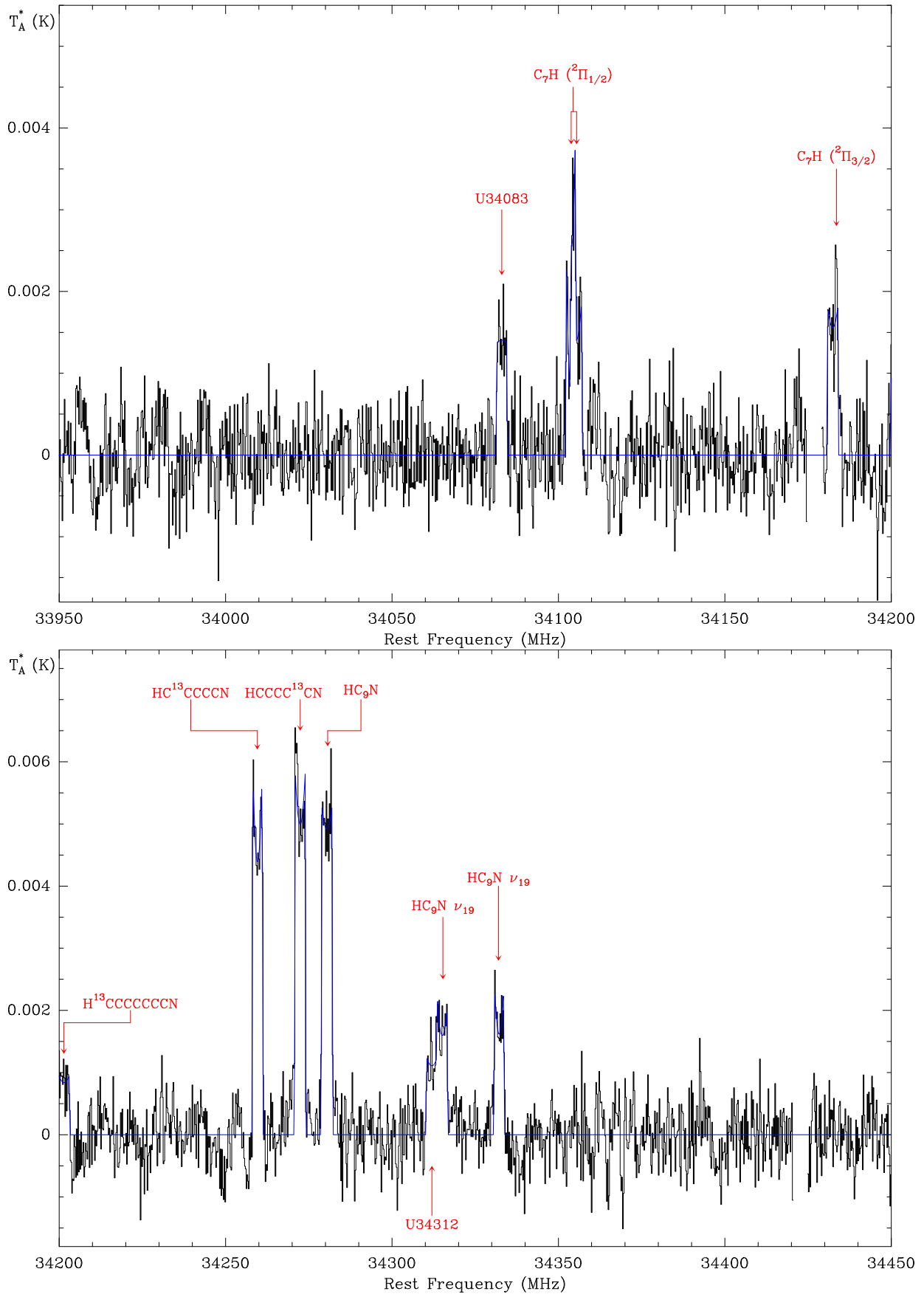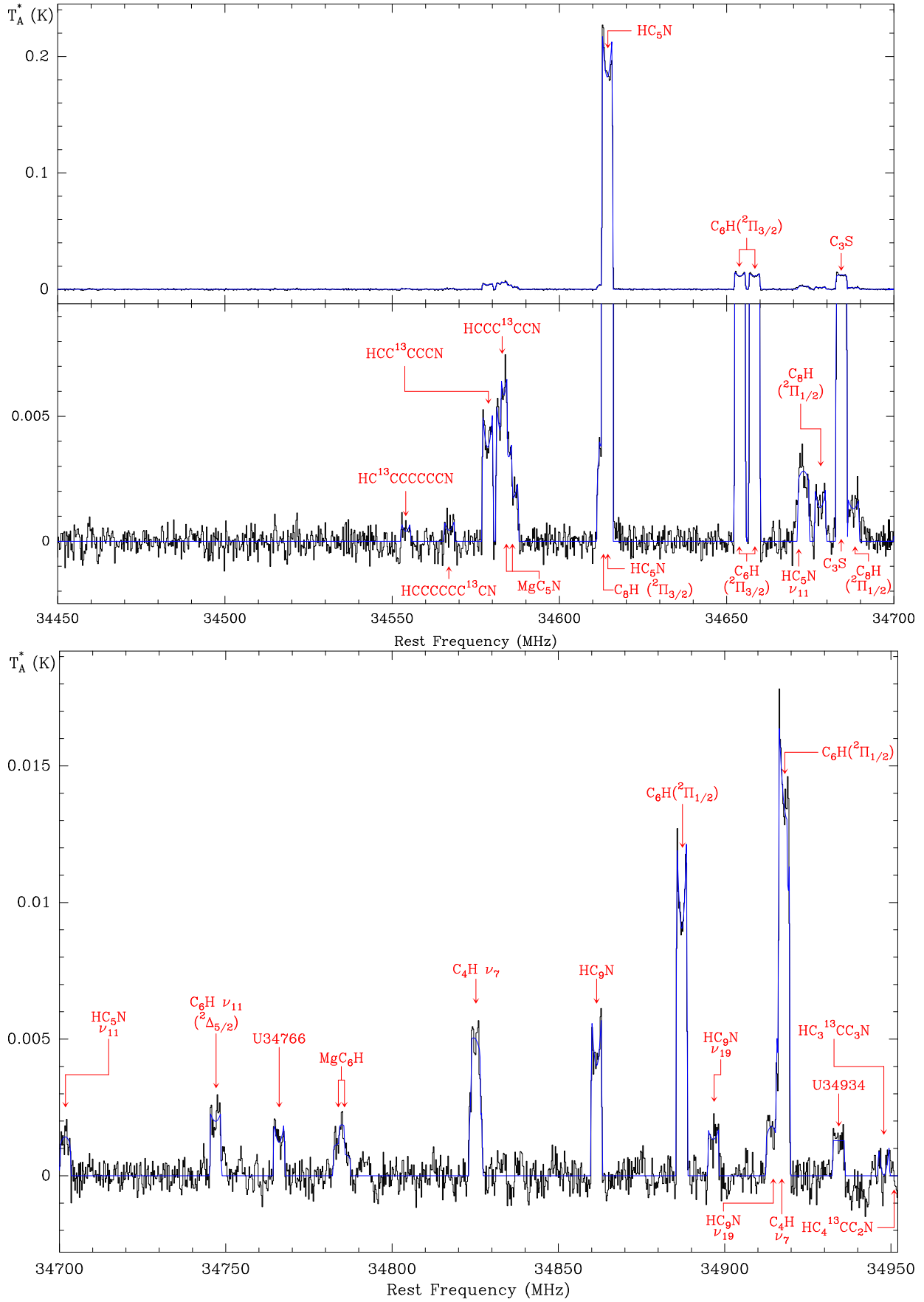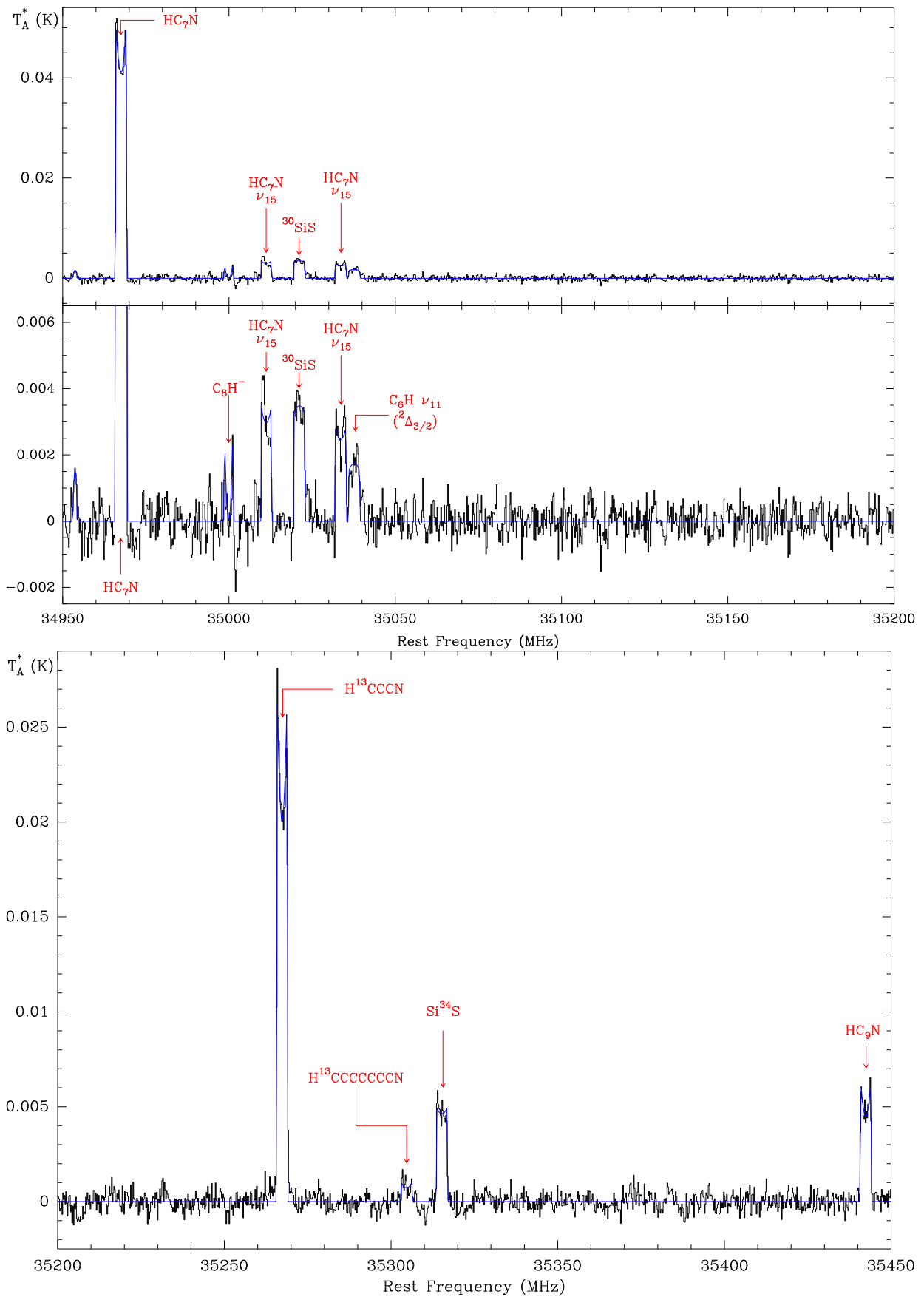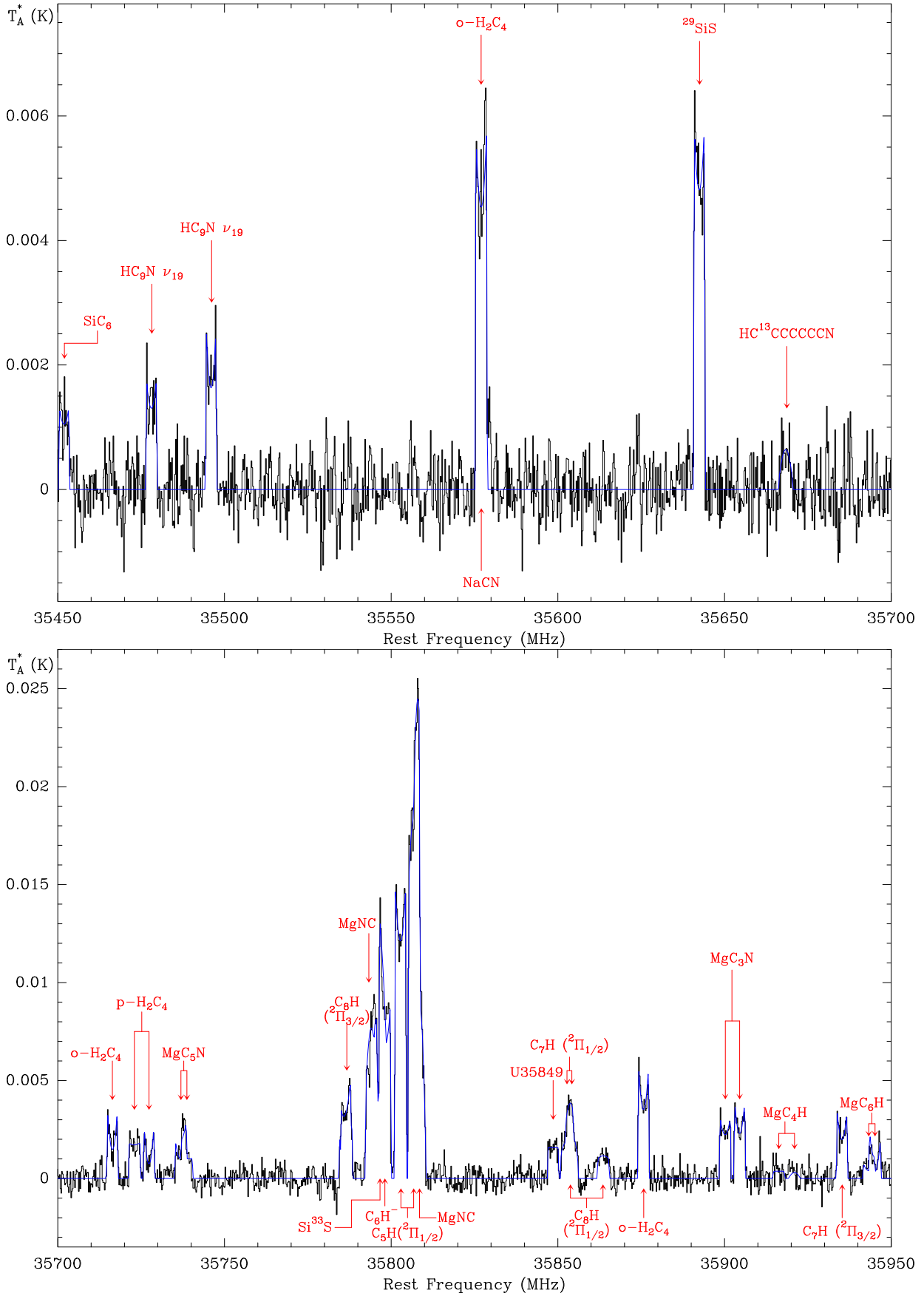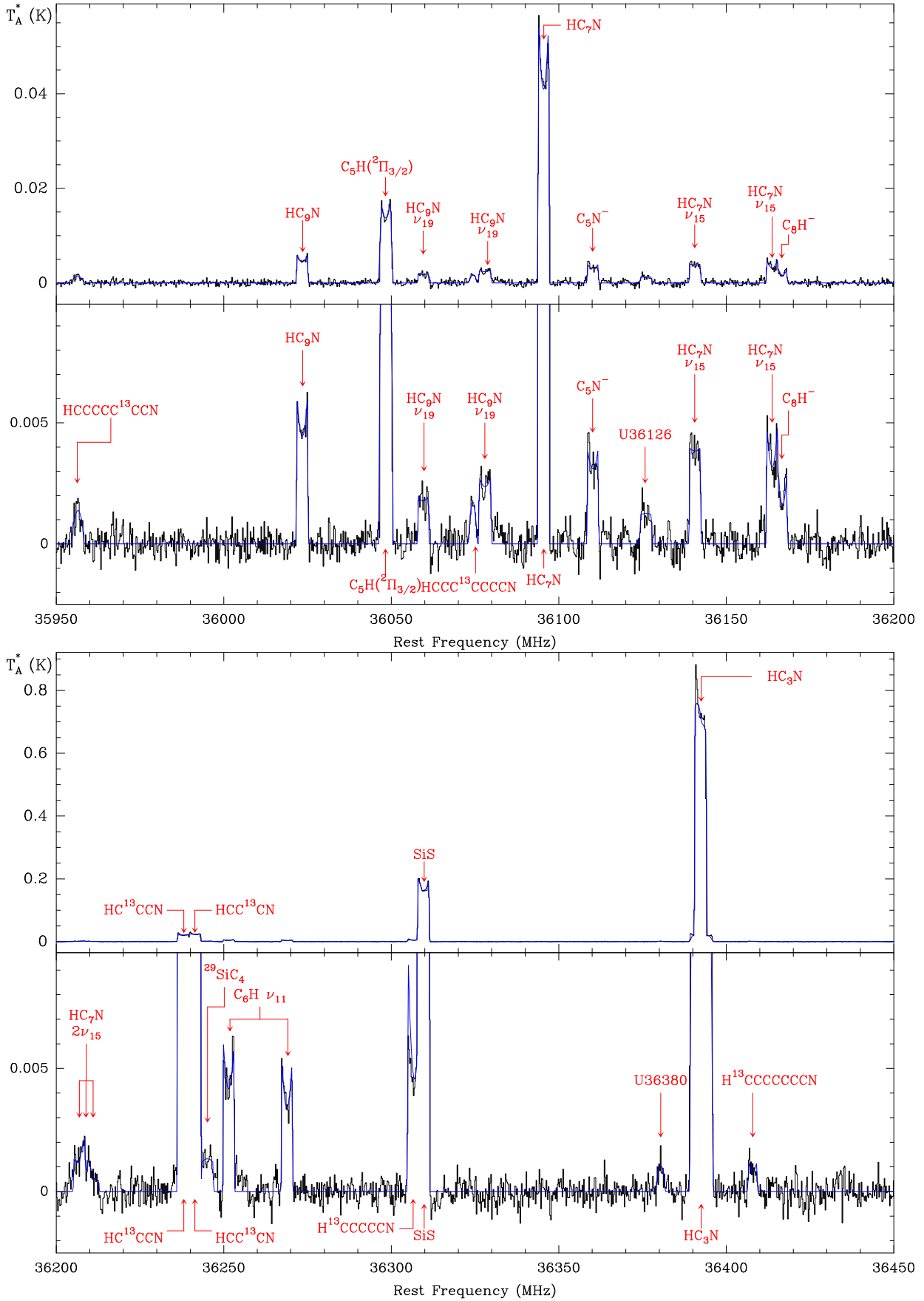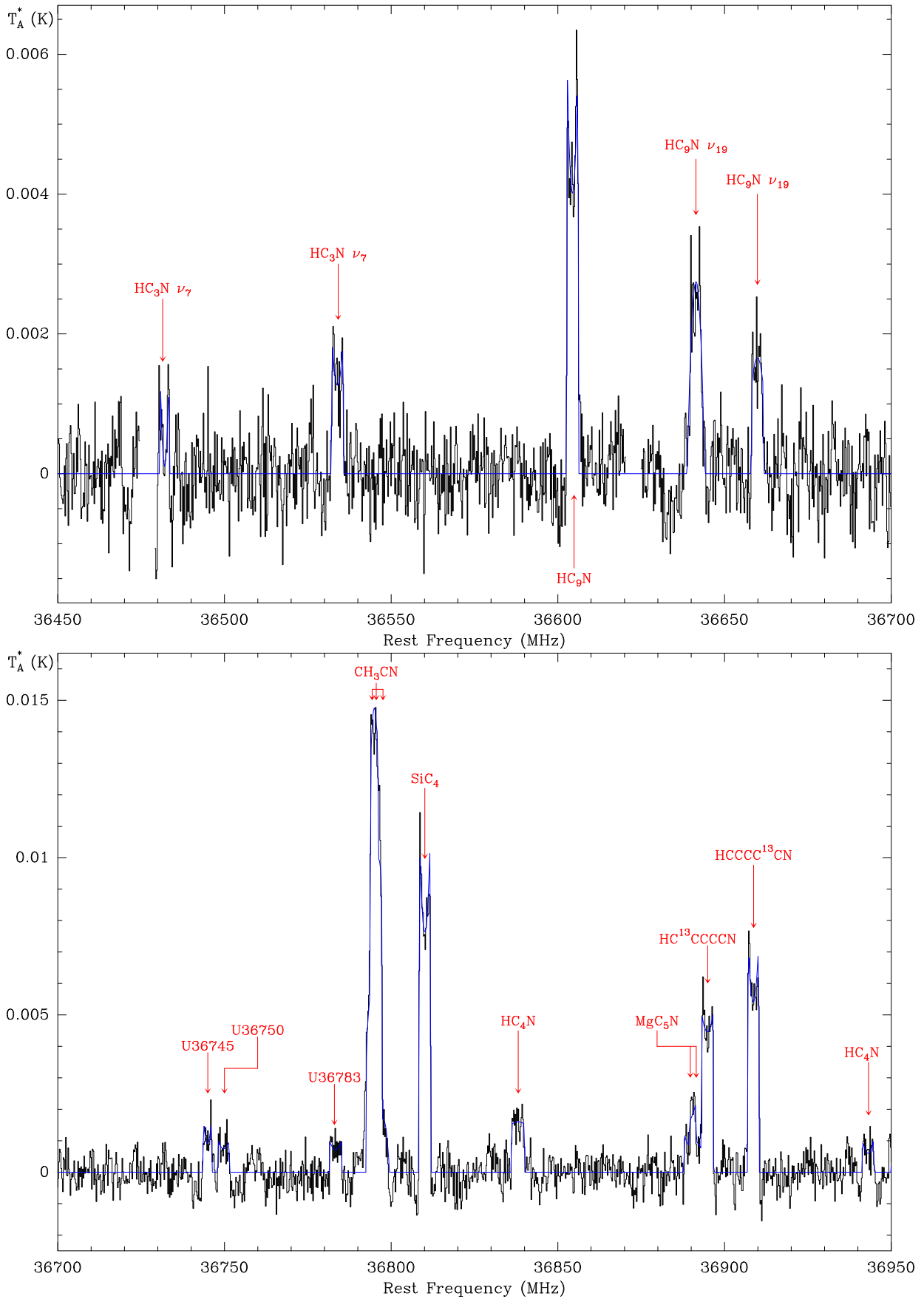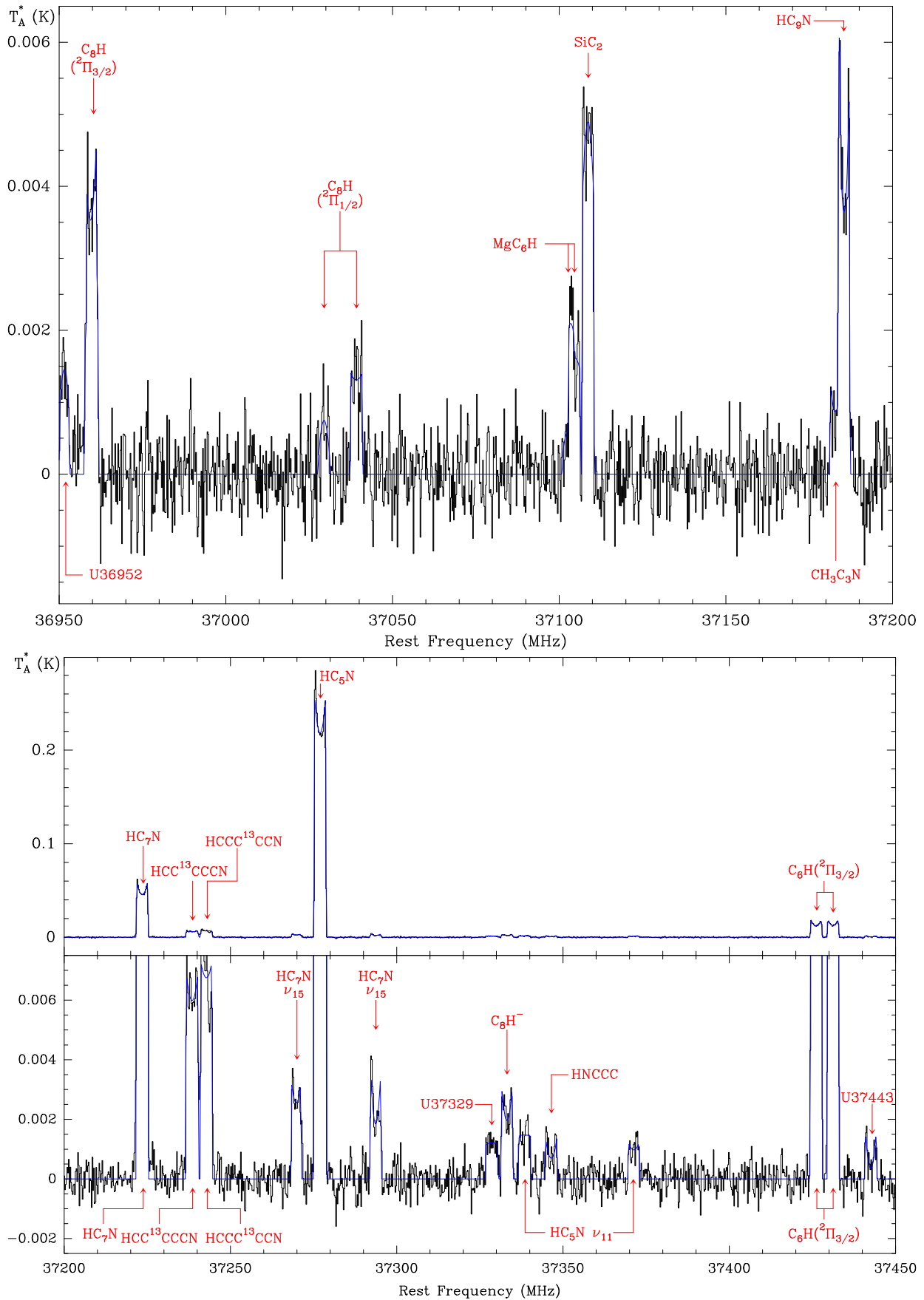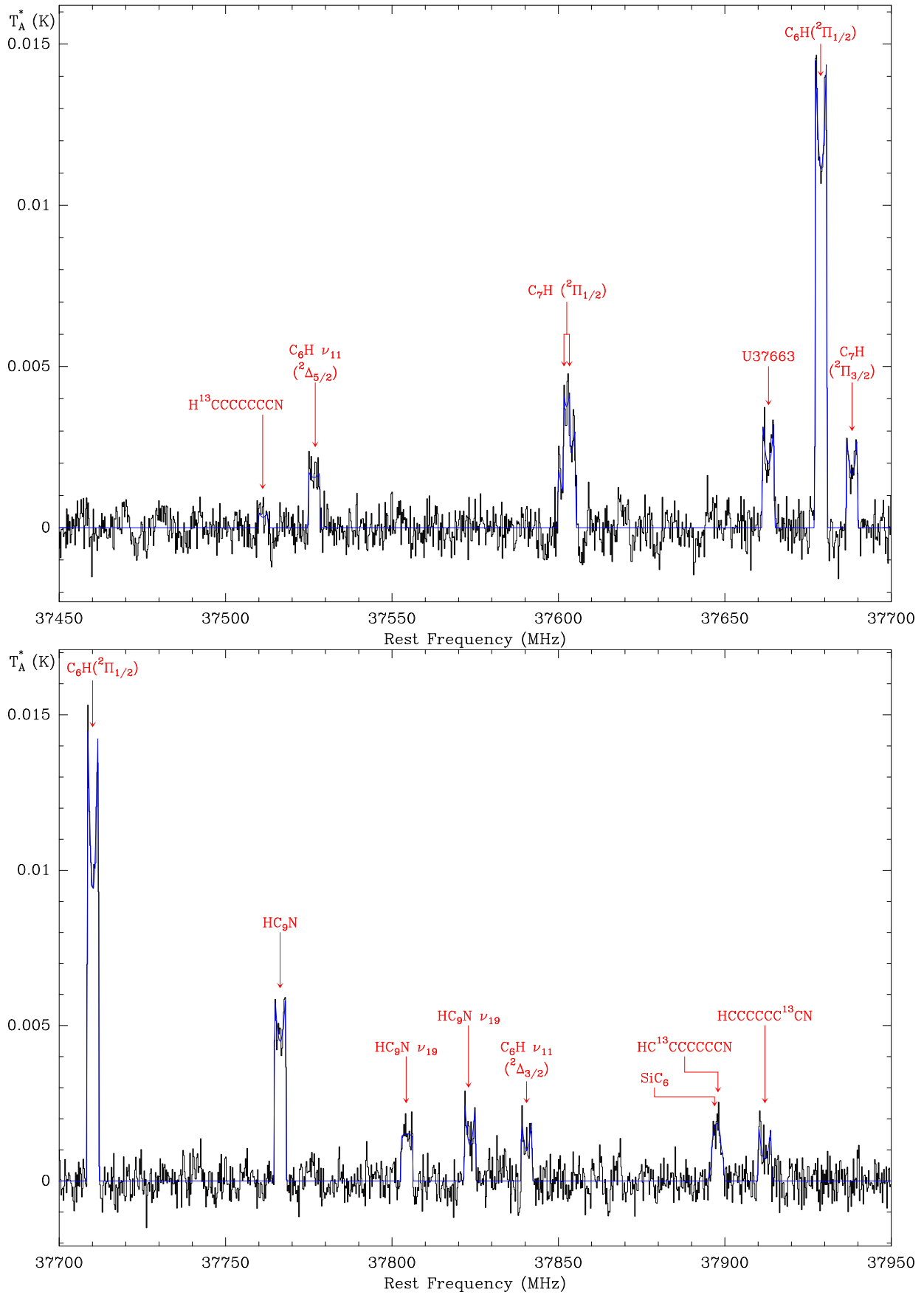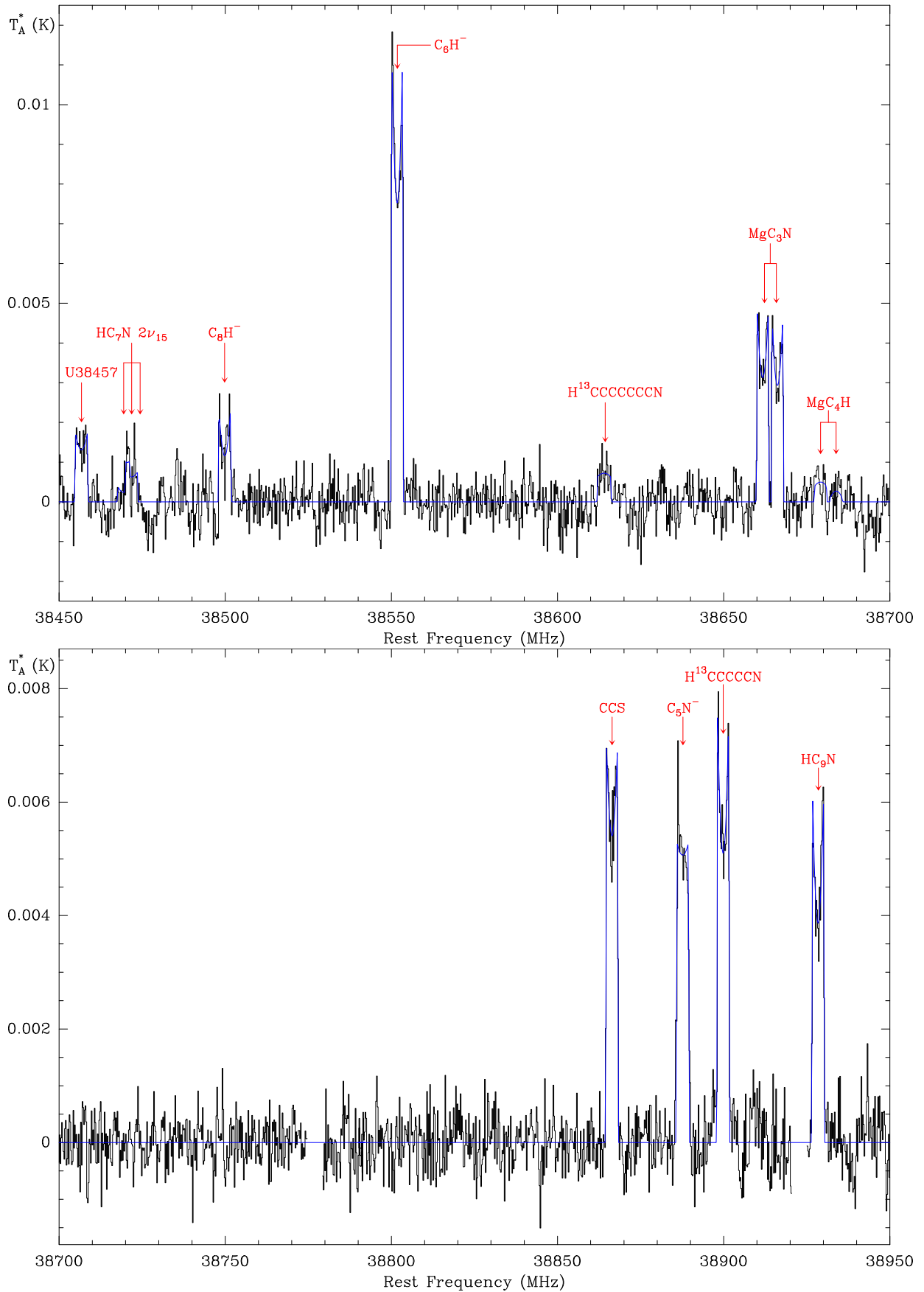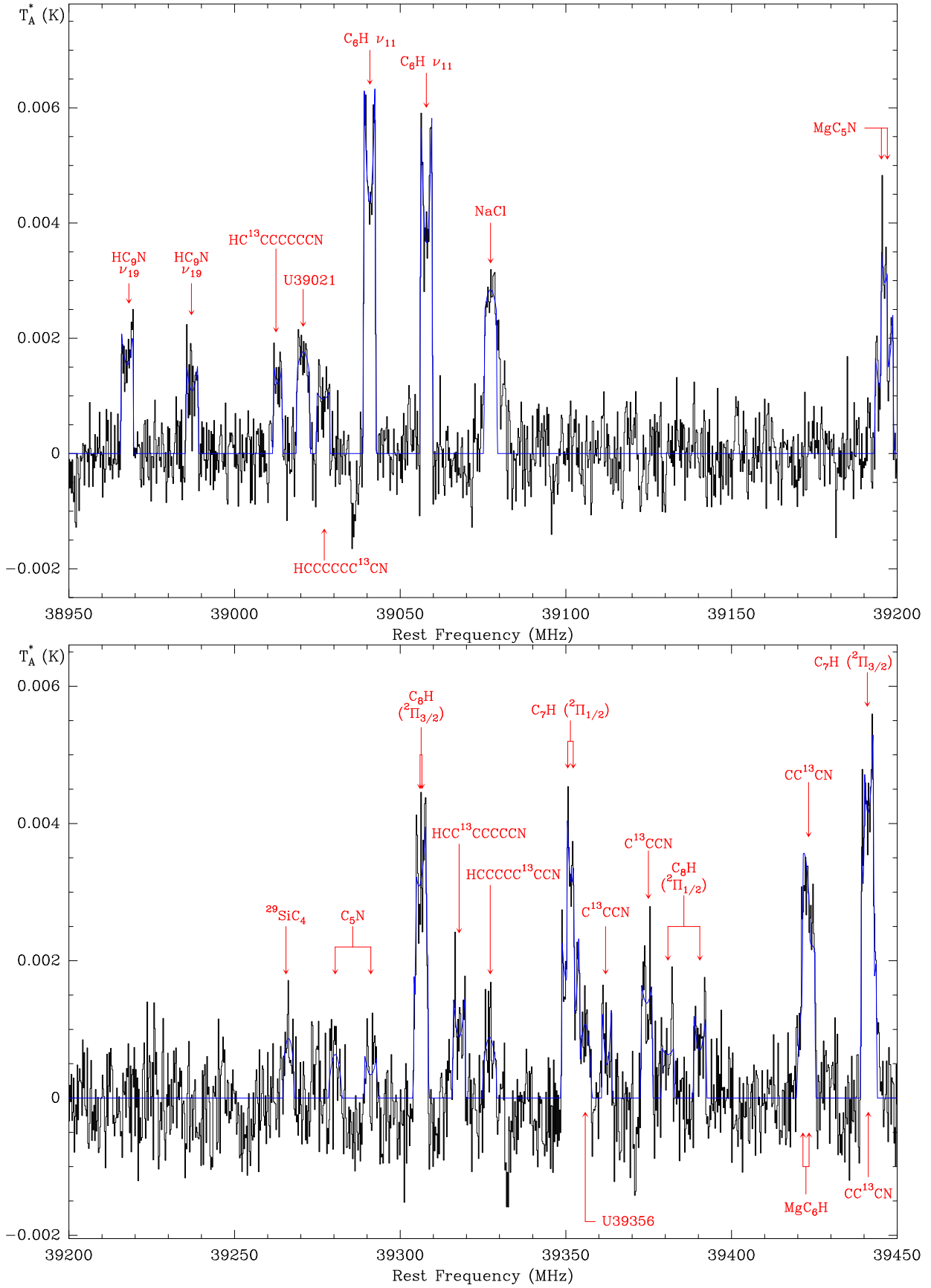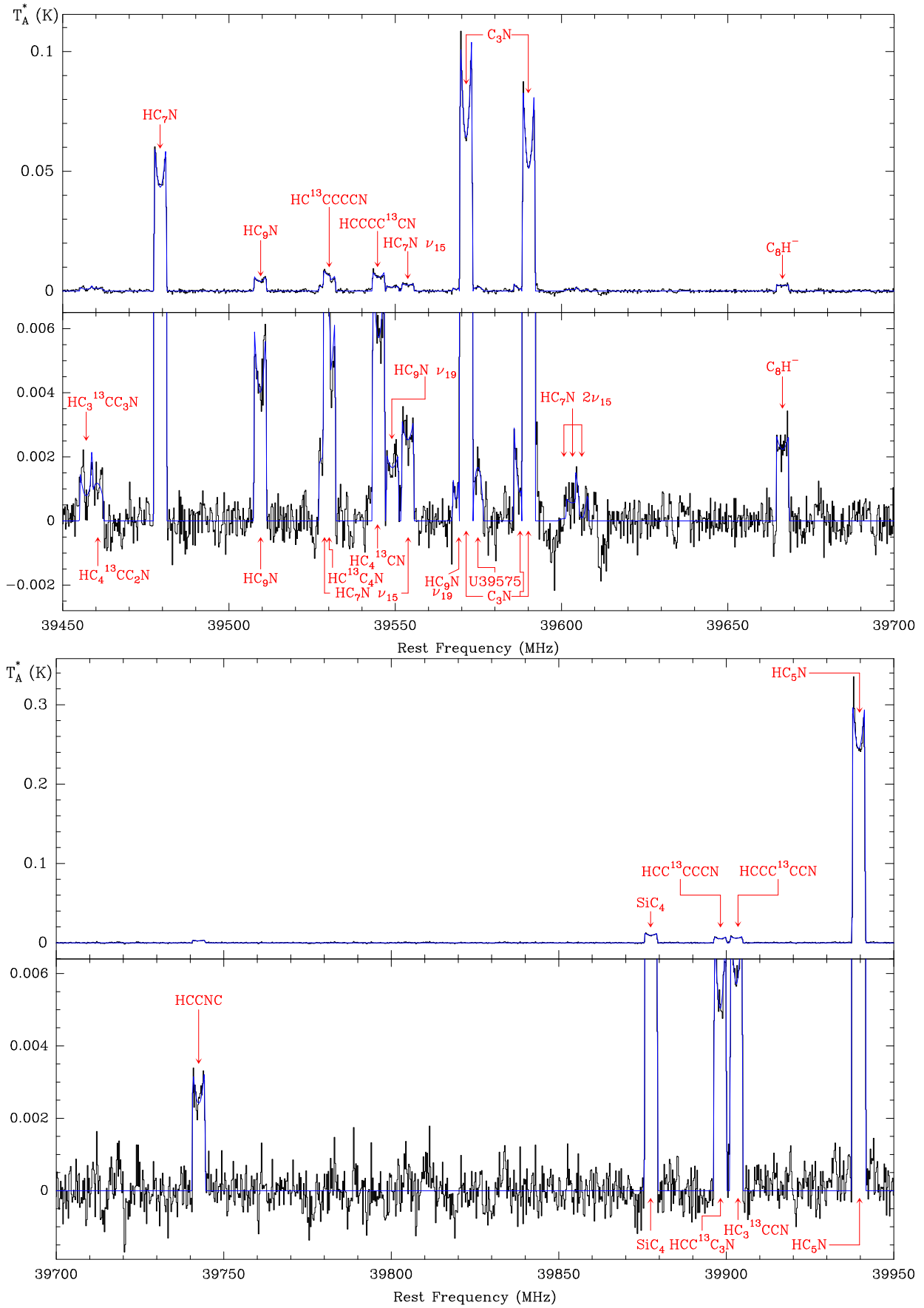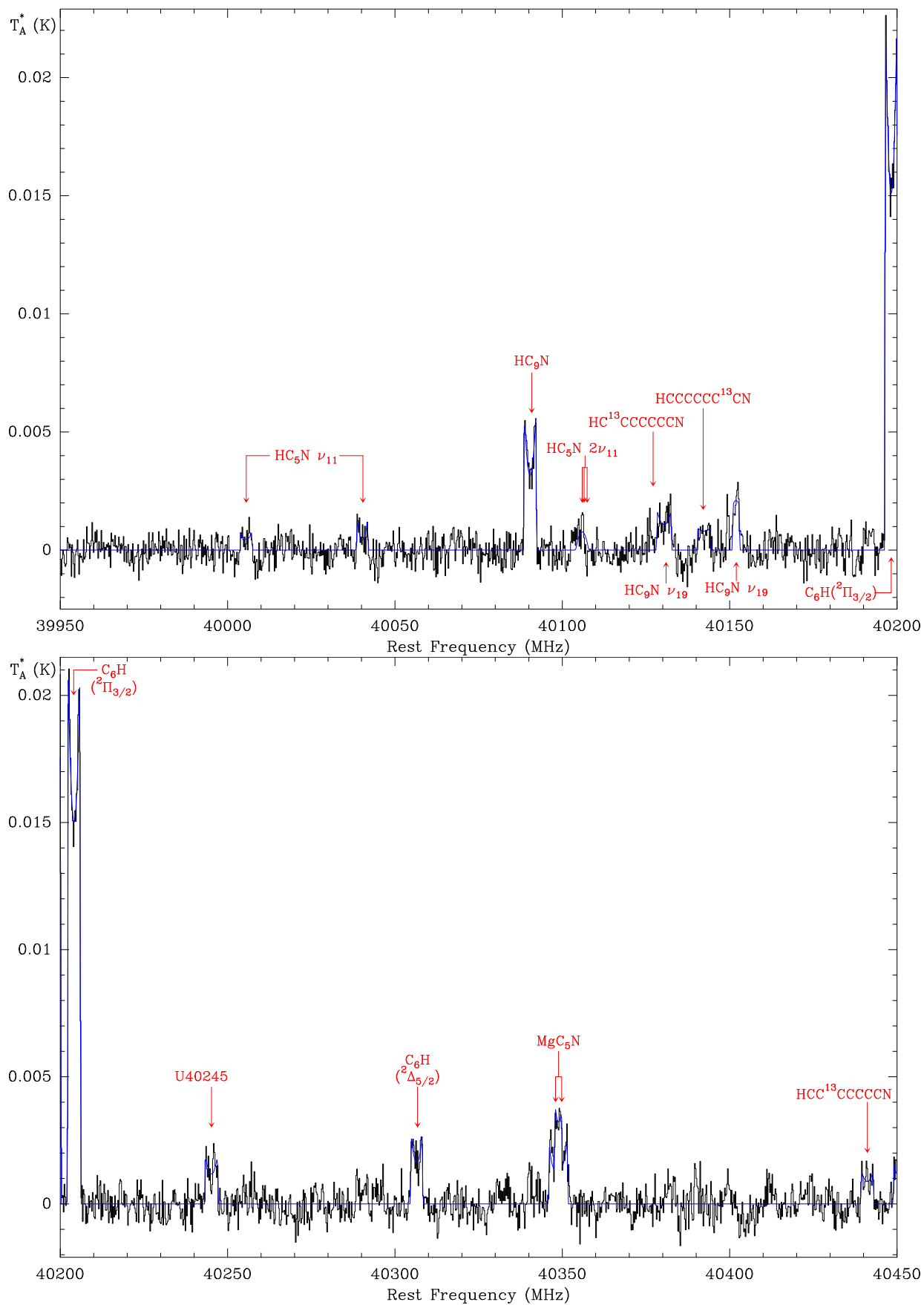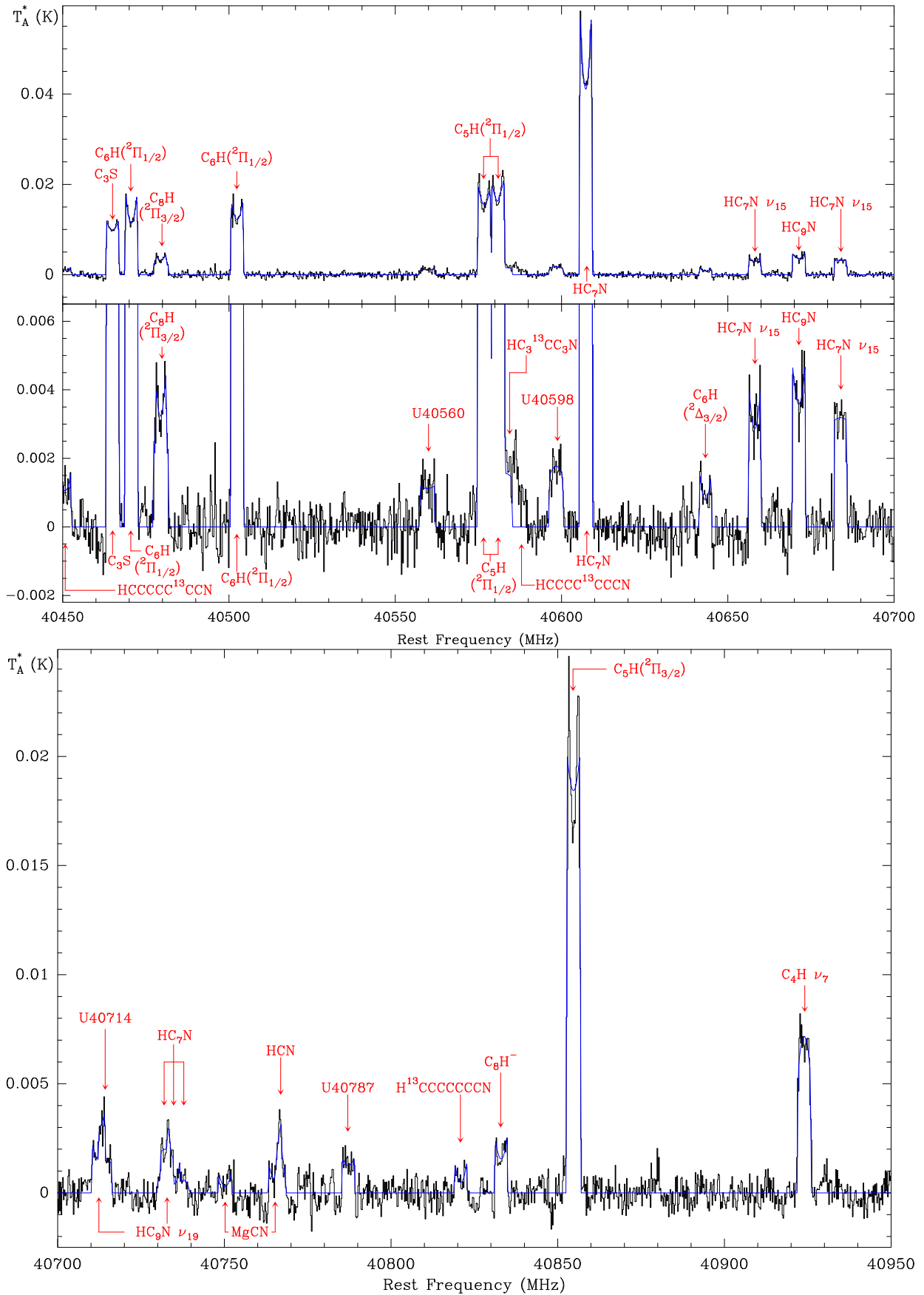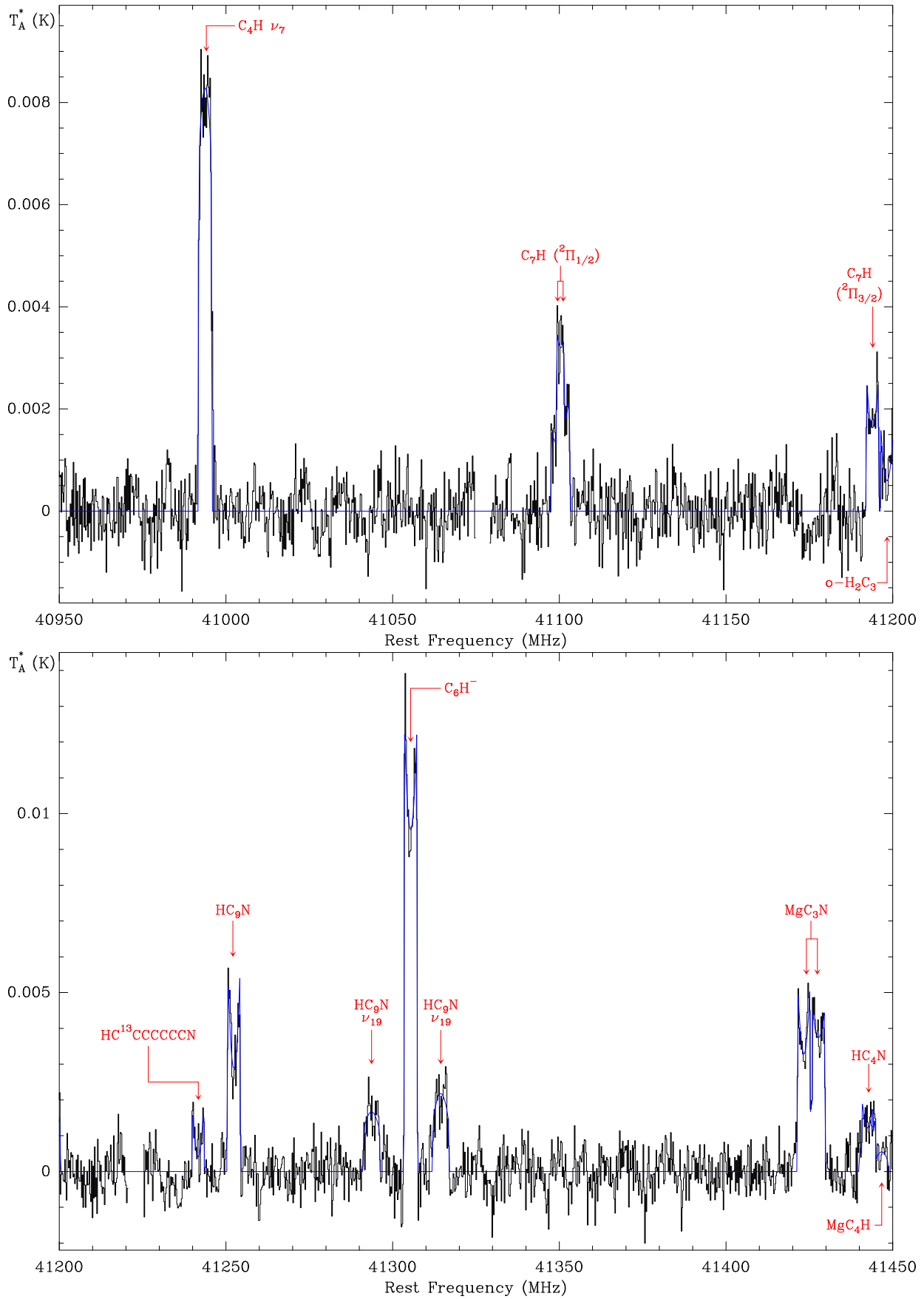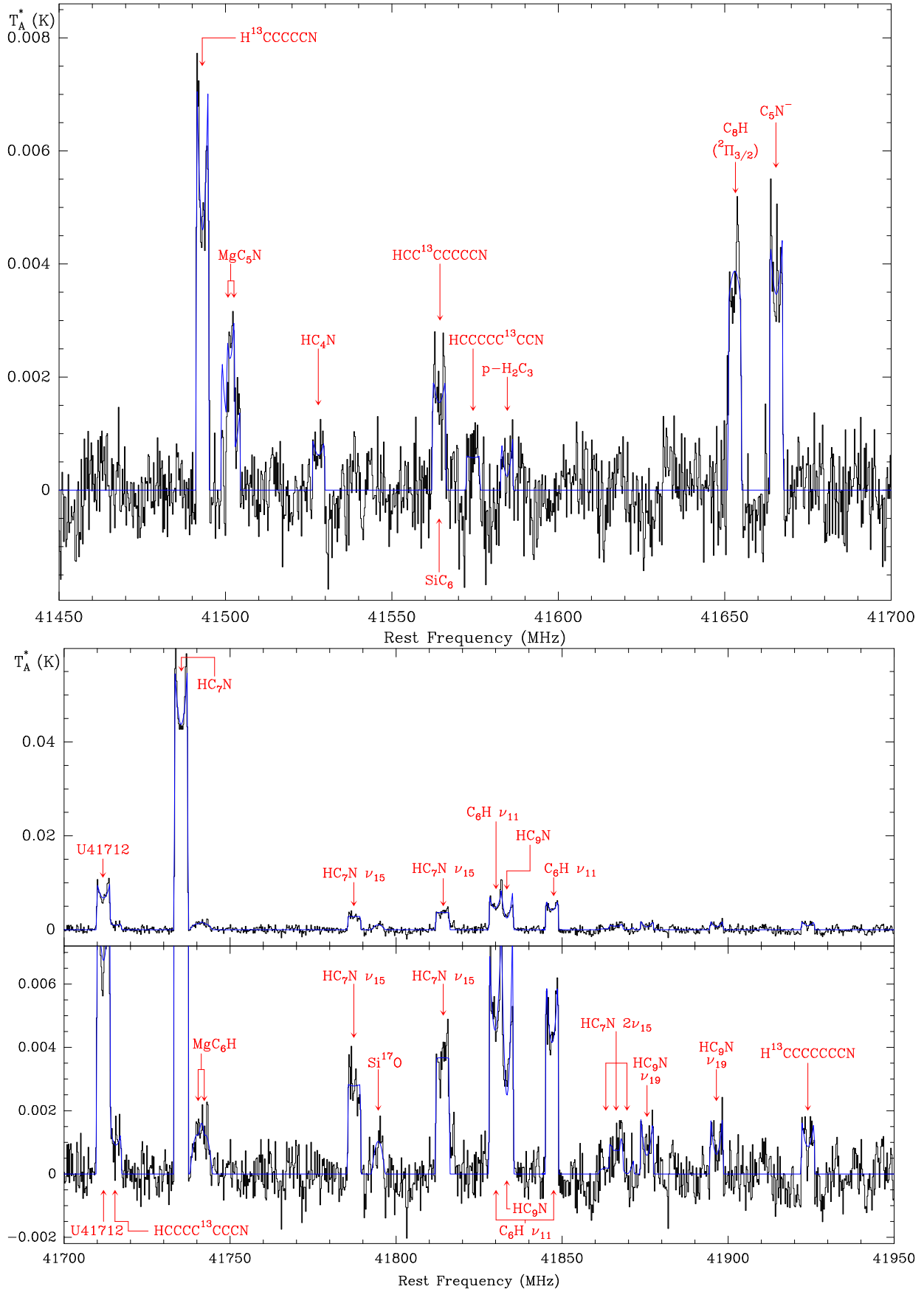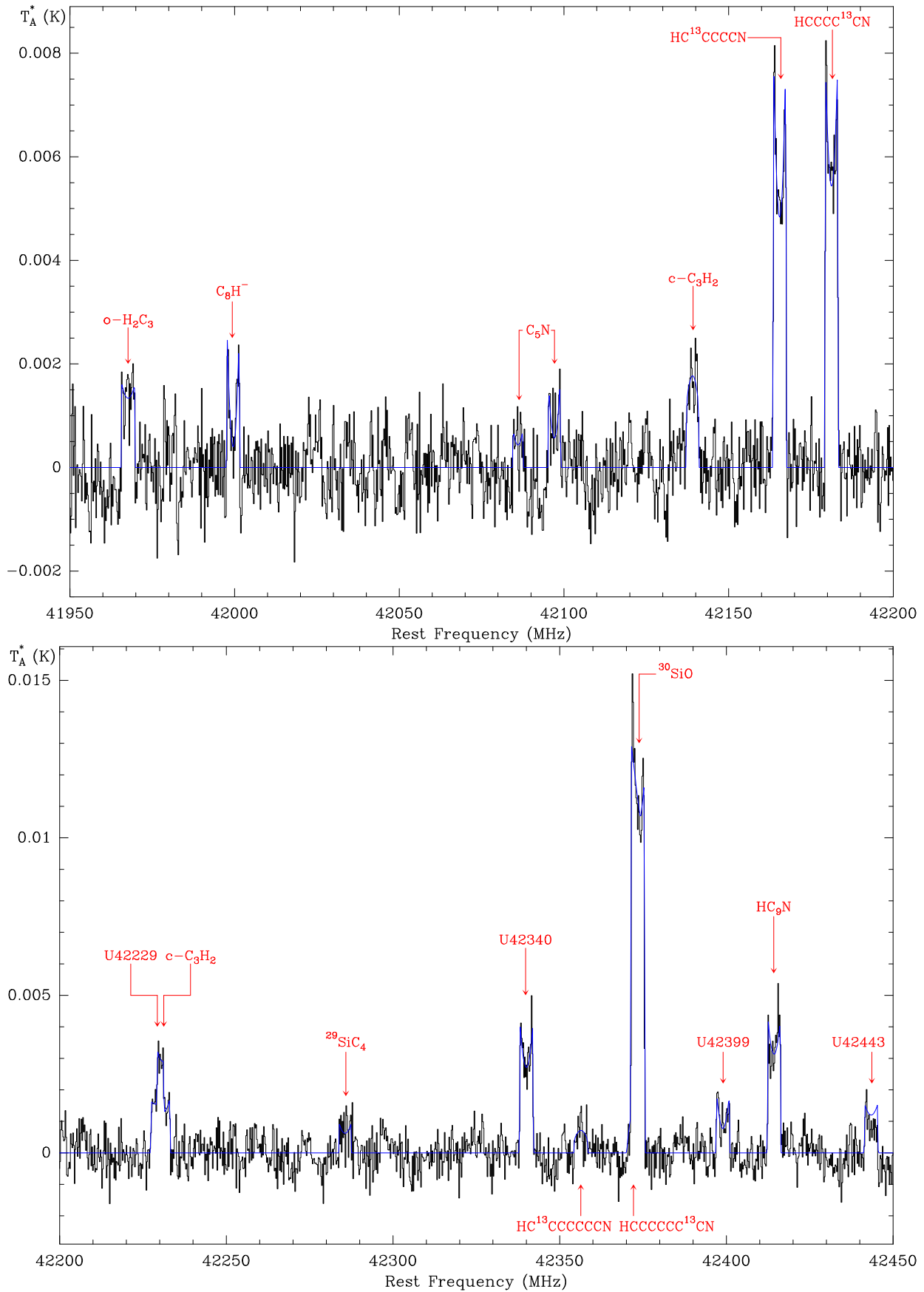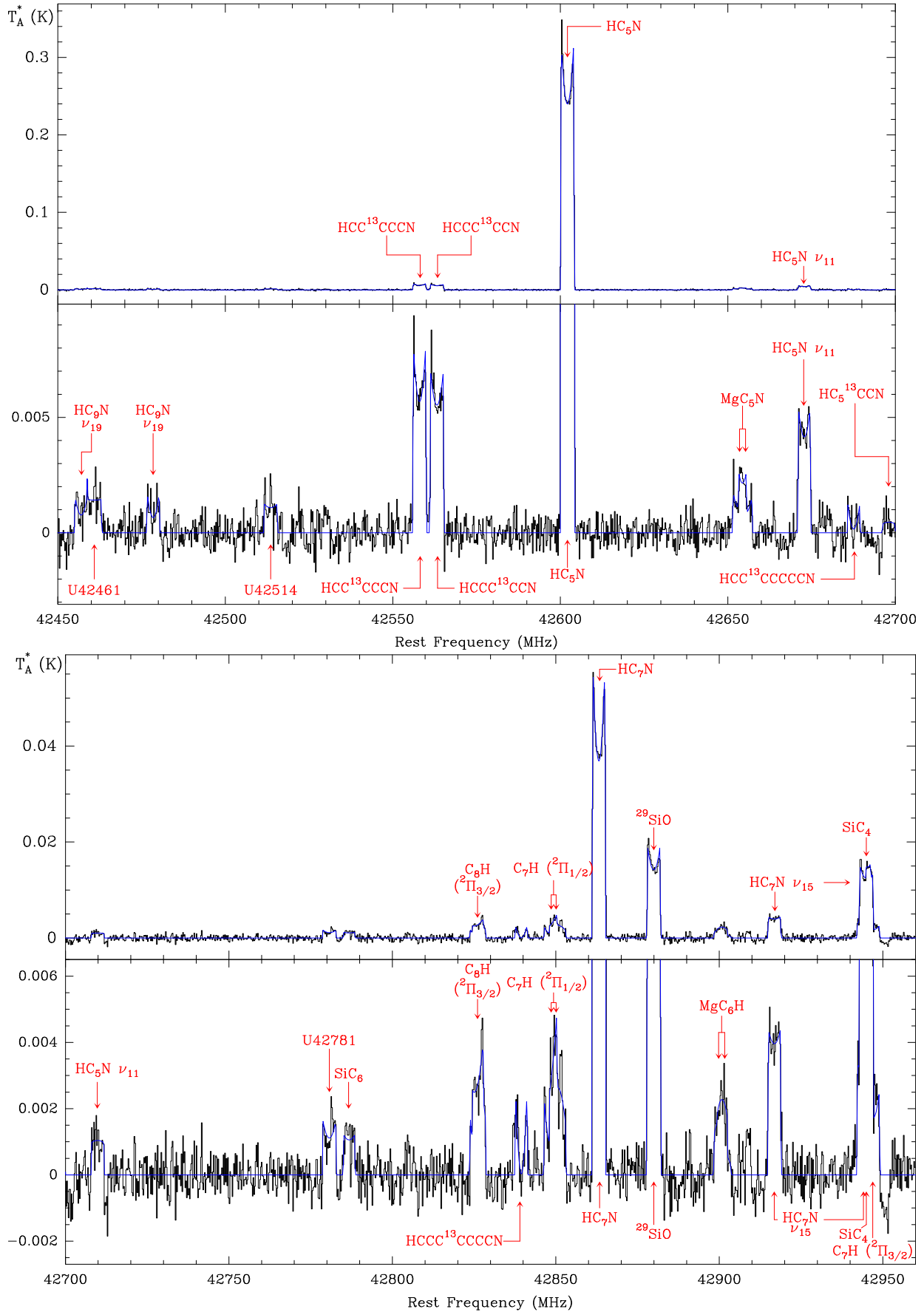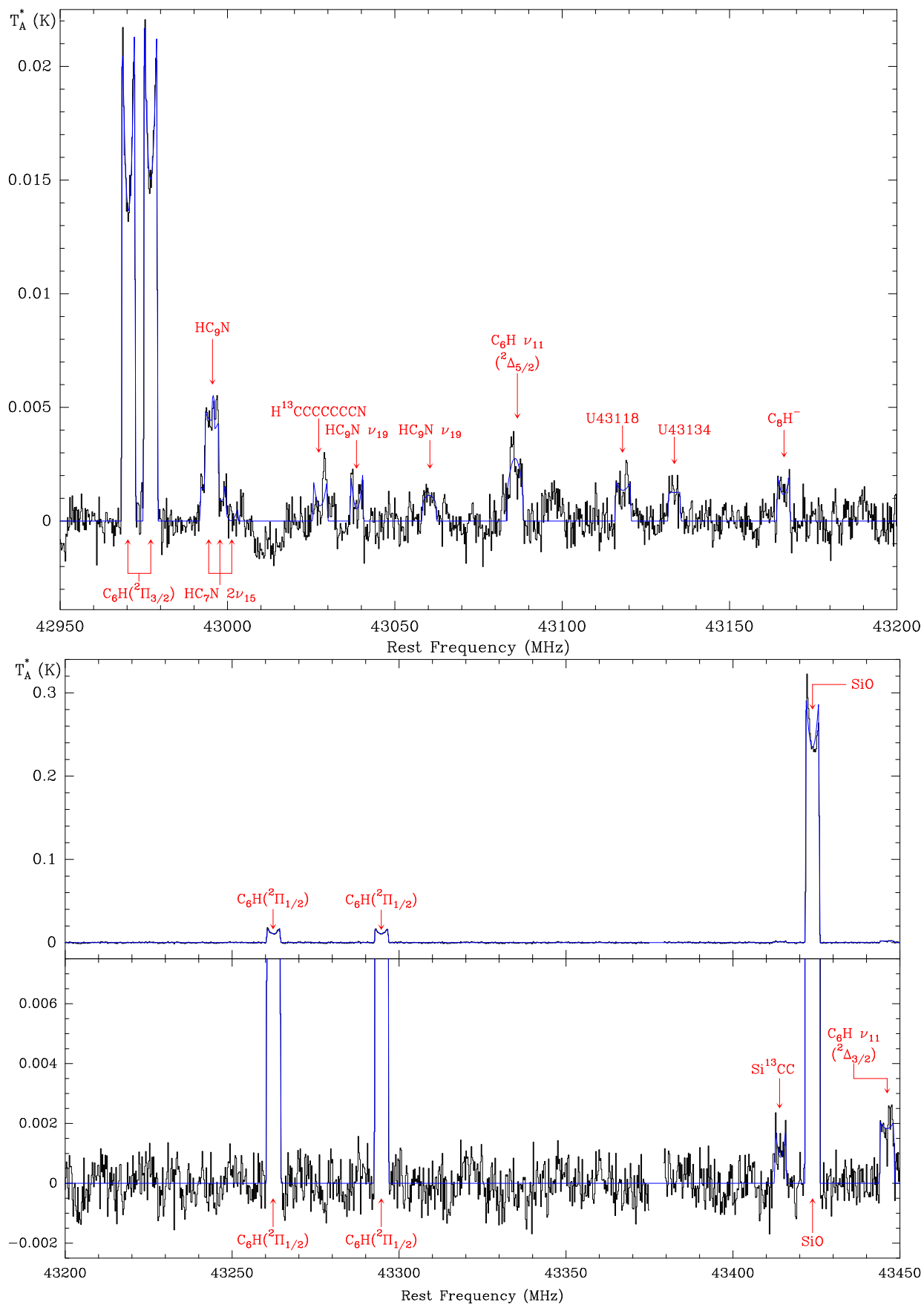**Fig. A.4.** IRC+10216 Yebes-40m data, line fits, and labels from 32450 to 32950 GHz.

Fig. A.5. IRC+10216 Yebes-40m data, line fits, and labels from 32950 to 33450 GHz.
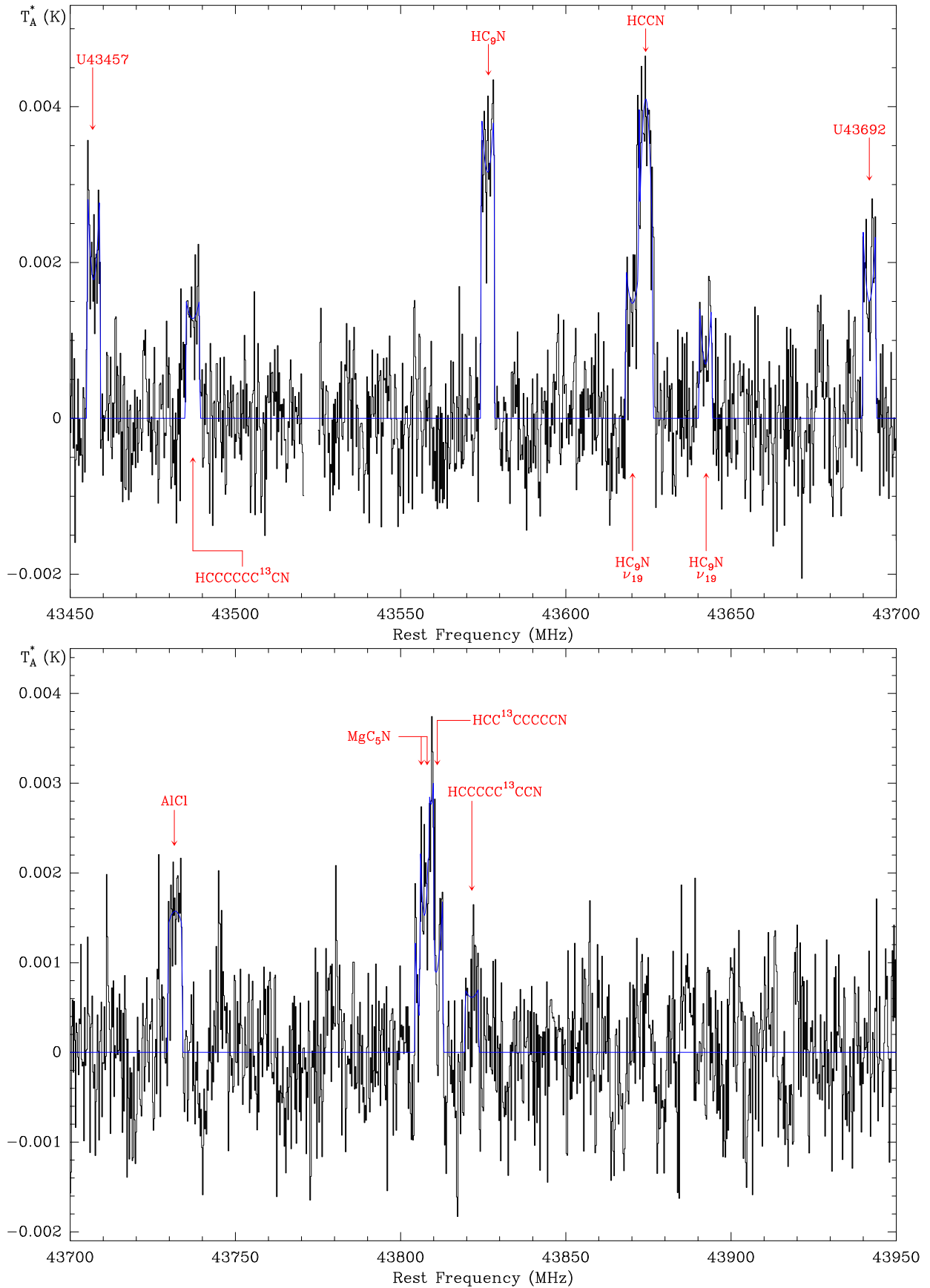
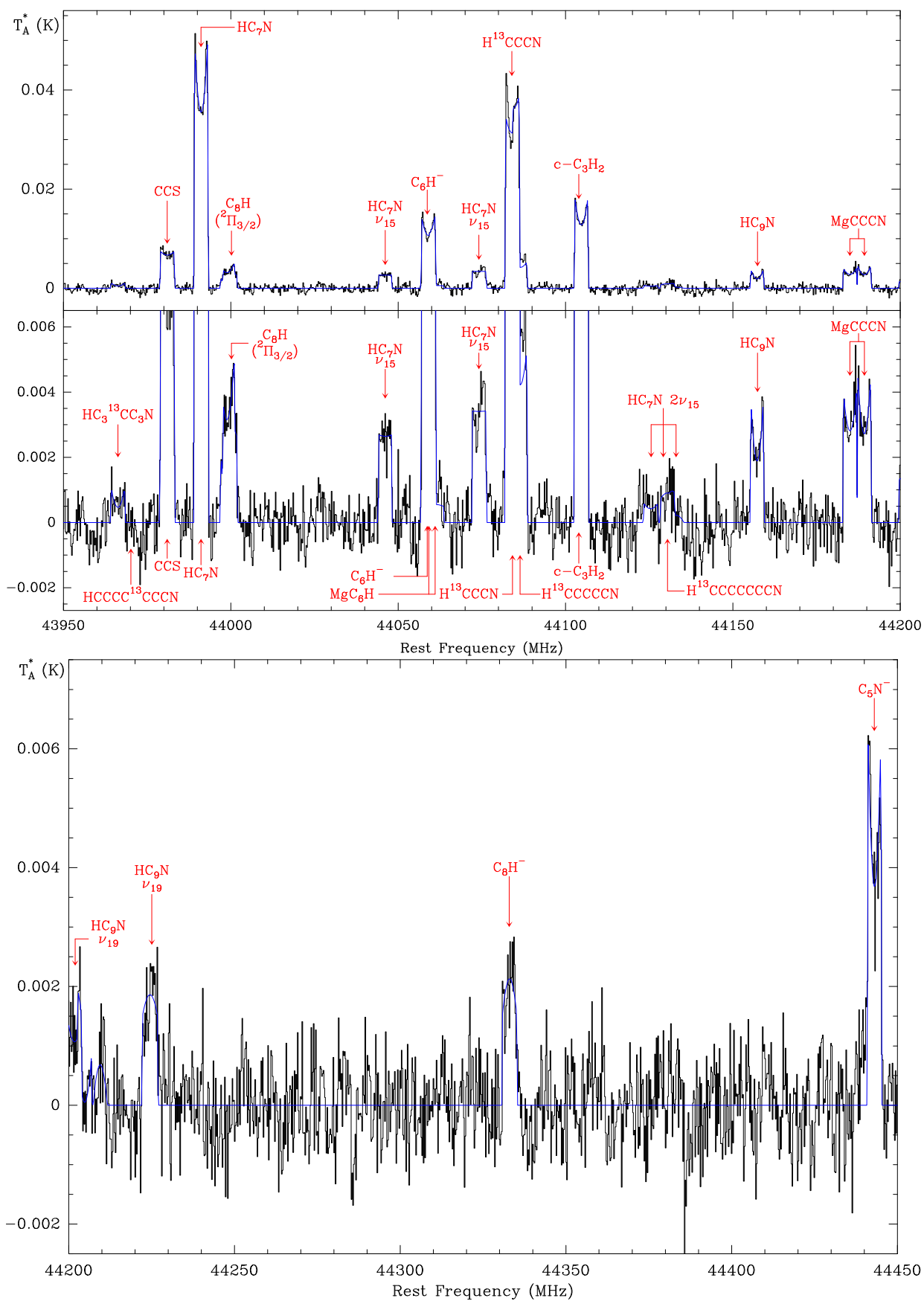**Fig. A.6.** IRC+10216 Yebes-40m data, line fits, and labels from 33450 to 33950 GHz.

Fig. A.7. IRC+10216 Yebes-40m data, line fits, and labels from 33950 to 34450 GHz.
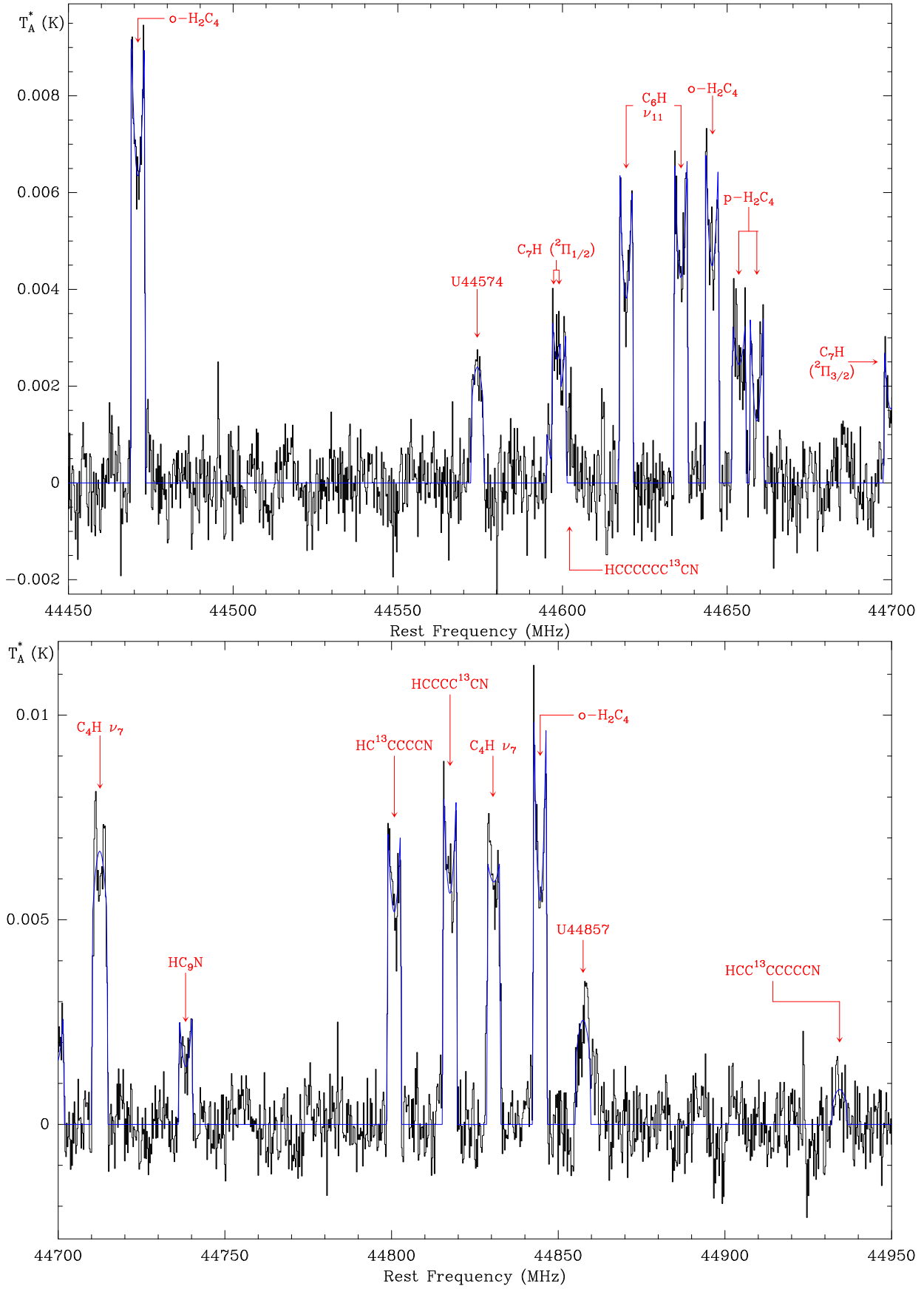
Fig. A.8. IRC+10216 Yebes-40m data, line fits, and labels from 34450 to 34950 GHz.

Fig. A.9. IRC+10216 Yebes-40m data, line fits, and labels from 34950 to 35450 GHz.

Fig. A.10. IRC+10216 Yebes-40m data, line fits, and labels from 35450 to 35950 GHz.

Fig. A.11. IRC+10216 Yebes-40m data, line fits, and labels from 35950 to 36450 GHz.

Fig. A.12. IRC+10216 Yebes-40m data, line fits, and labels from 36450 to 36950 GHz.
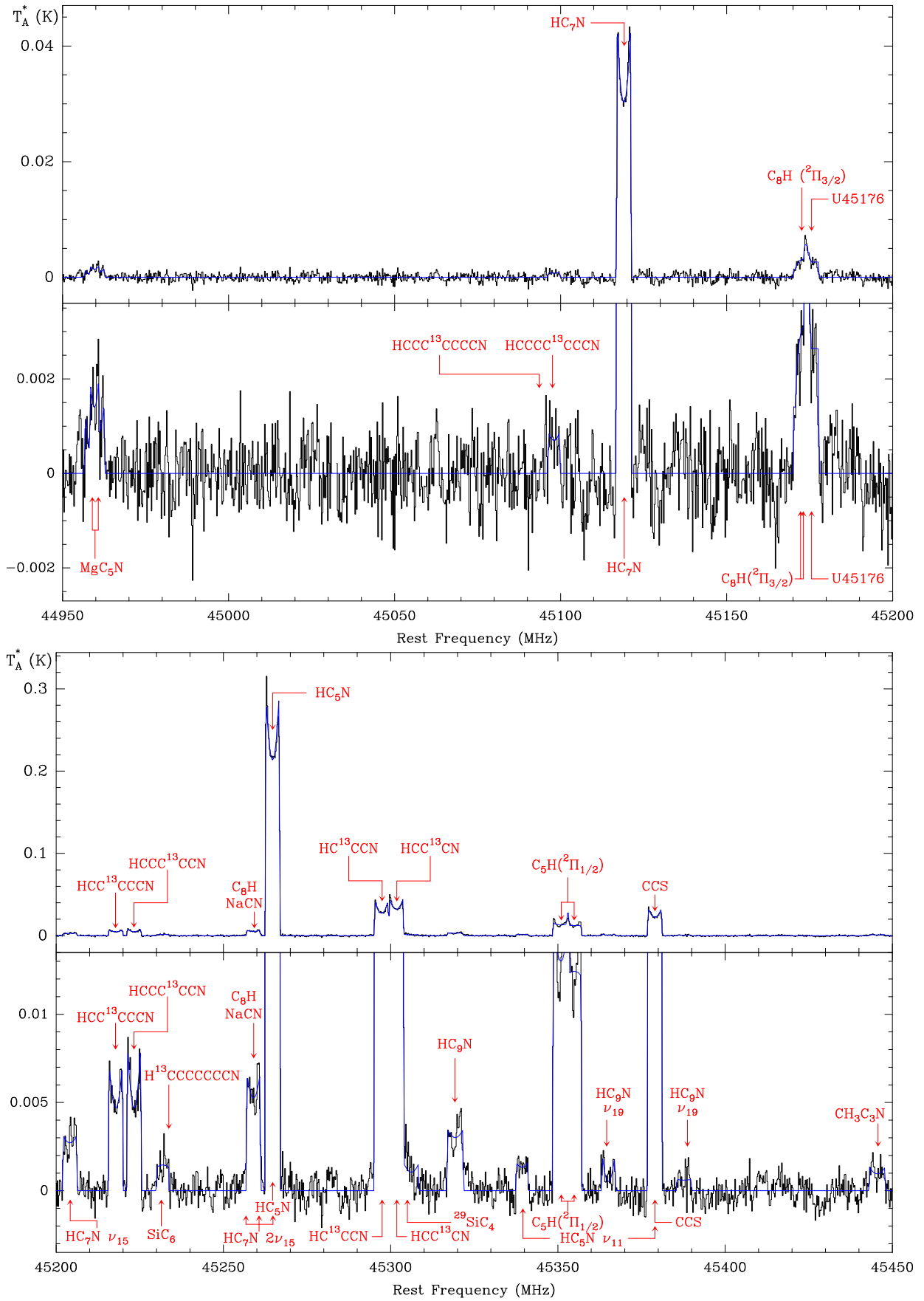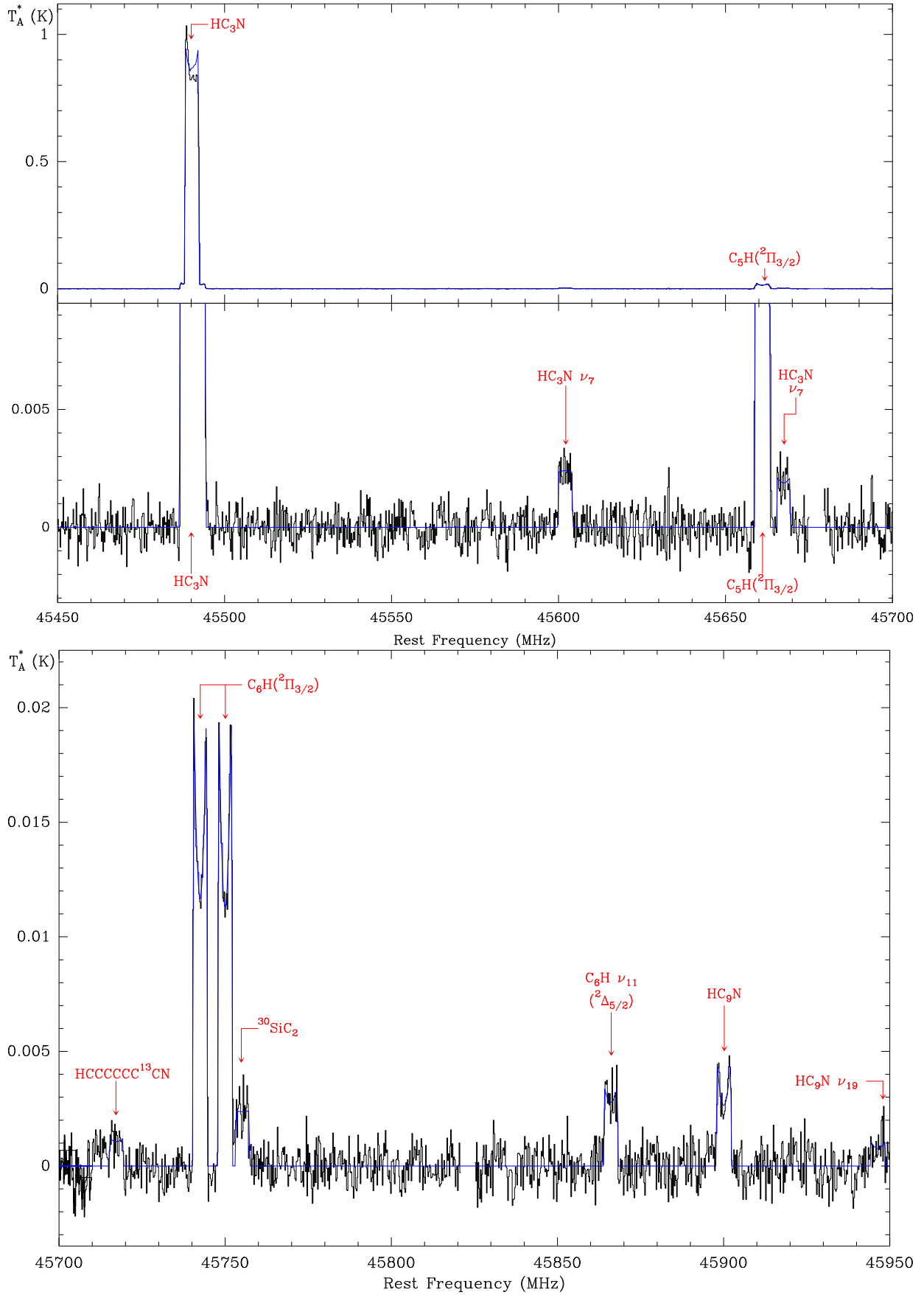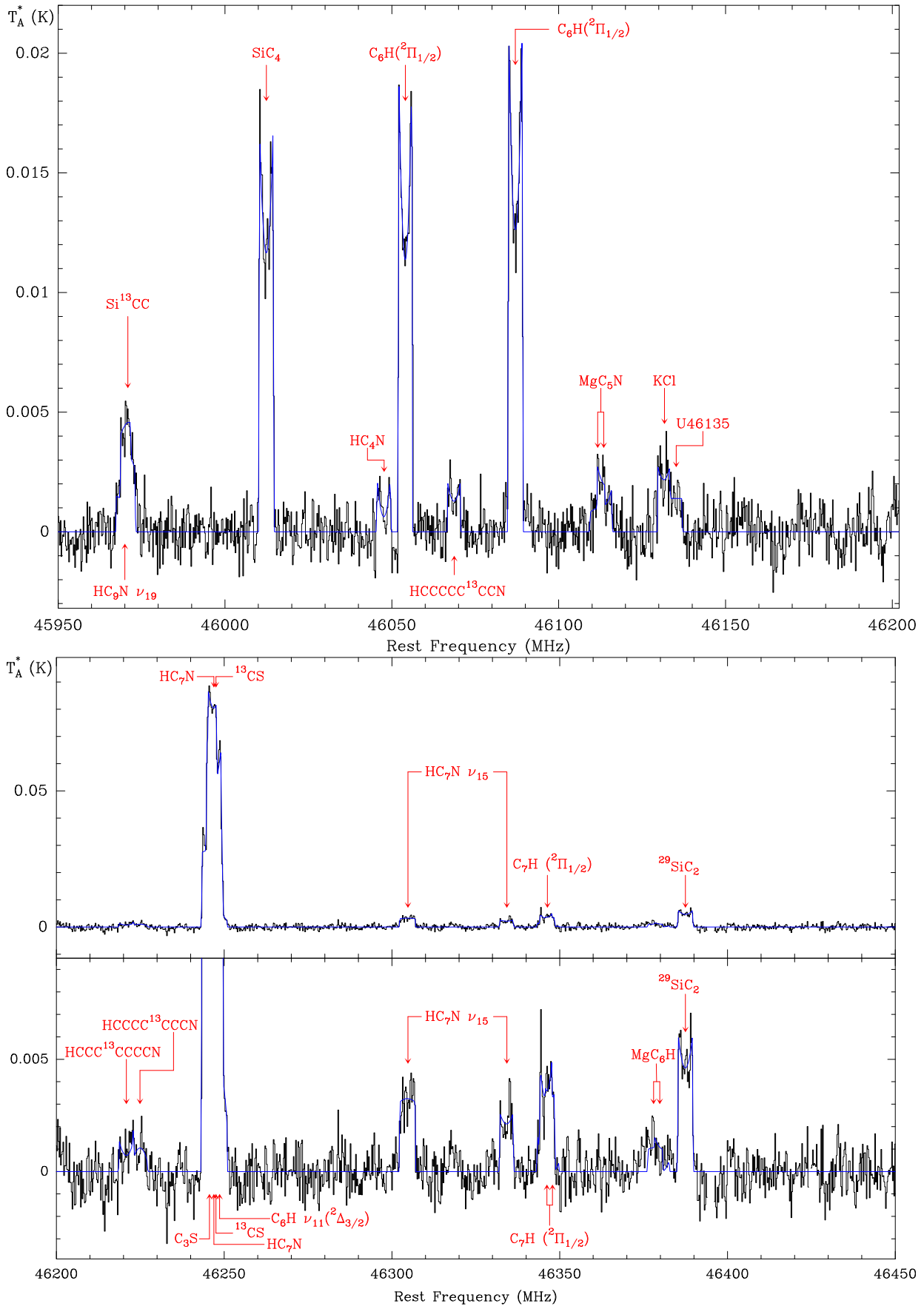
Fig. A.13. IRC+10216 Yebes-40m data, line fits, and labels from 36950 to 37450 GHz.

Fig. A.14. IRC+10216 Yebes-40m data, line fits, and labels from 37450 to 37950 GHz.

Fig. A.15. IRC+10216 Yebes-40m data, line fits, and labels from 37950 to 38450 GHz.

Fig. A.16. IRC+10216 Yebes-40m data, line fits, and labels from 38450 to 38950 GHz.

Fig. A.17. IRC+10216 Yebes-40m data, line fits, and labels from 38950 to 39450 GHz.

Fig. A.18. IRC+10216 Yebes-40m data, line fits, and labels from 39450 to 39950 GHz.

Fig. A.19. IRC+10216 Yebes-40m data, line fits, and labels from 39950 to 40450 GHz.

Fig. A.20. IRC+10216 Yebes-40m data, line fits, and labels from 40450 to 40950 GHz.

Fig. A.21. IRC+10216 Yebes-40m data, line fits, and labels from 40950 to 41450 GHz.
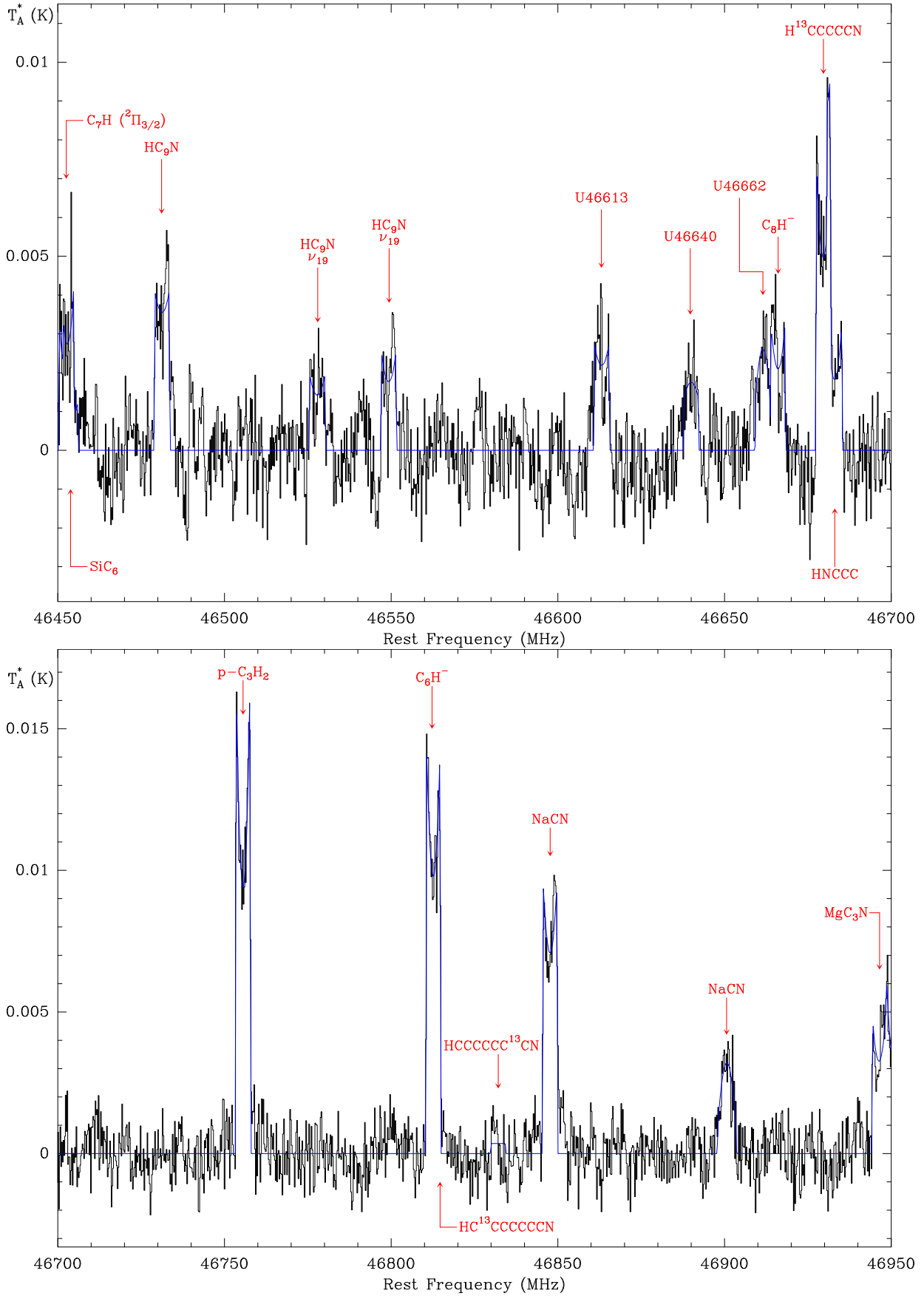
Fig. A.22. IRC+10216 Yebes-40m data, line fits, and labels from 41450 to 41950 GHz.
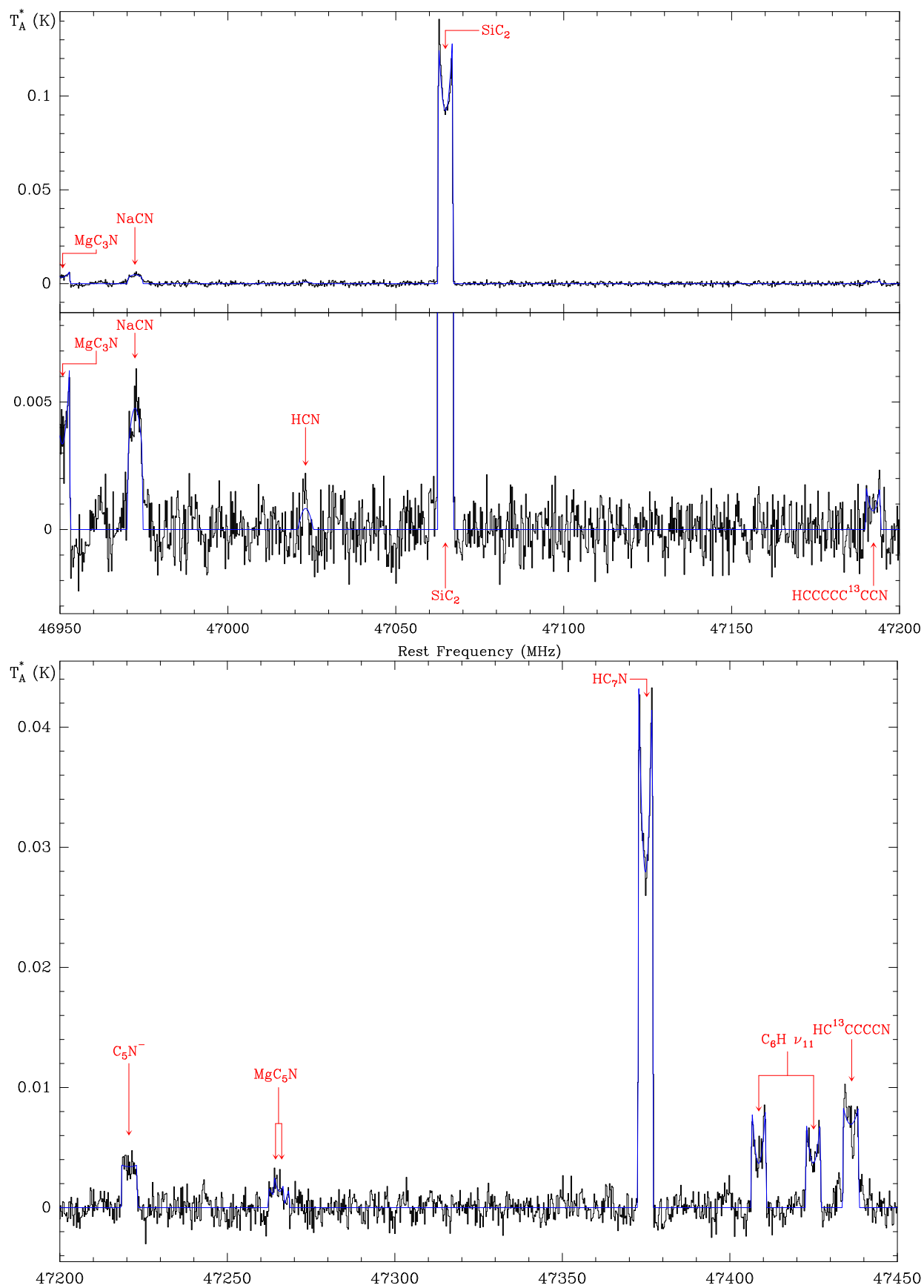
Fig. A.23. IRC+10216 Yebes-40m data, line fits, and labels from 41950 to 42450 GHz.
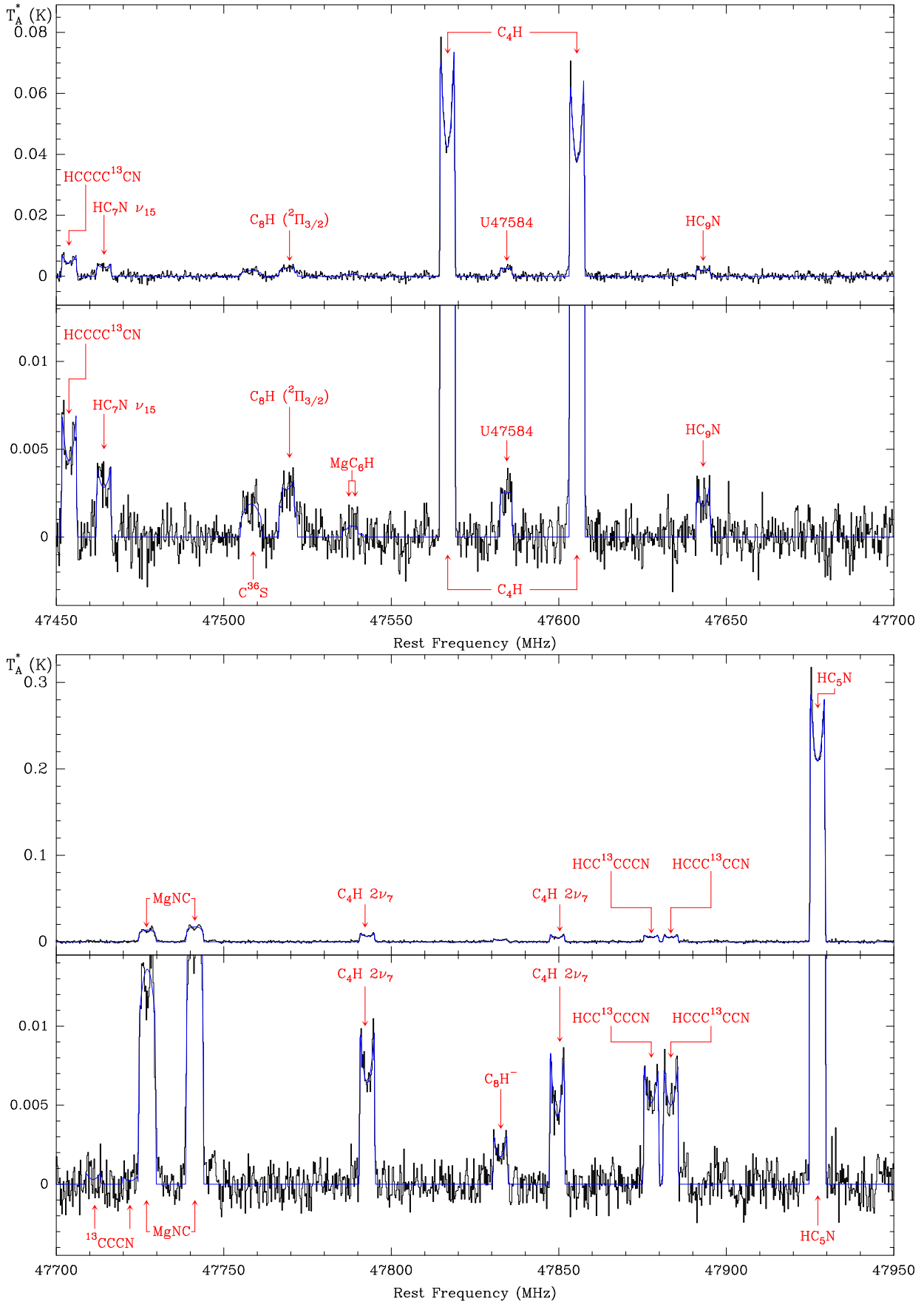
Fig. A.24. IRC+10216 Yebes-40m data, line fits, and labels from 42450 to 42950 GHz.
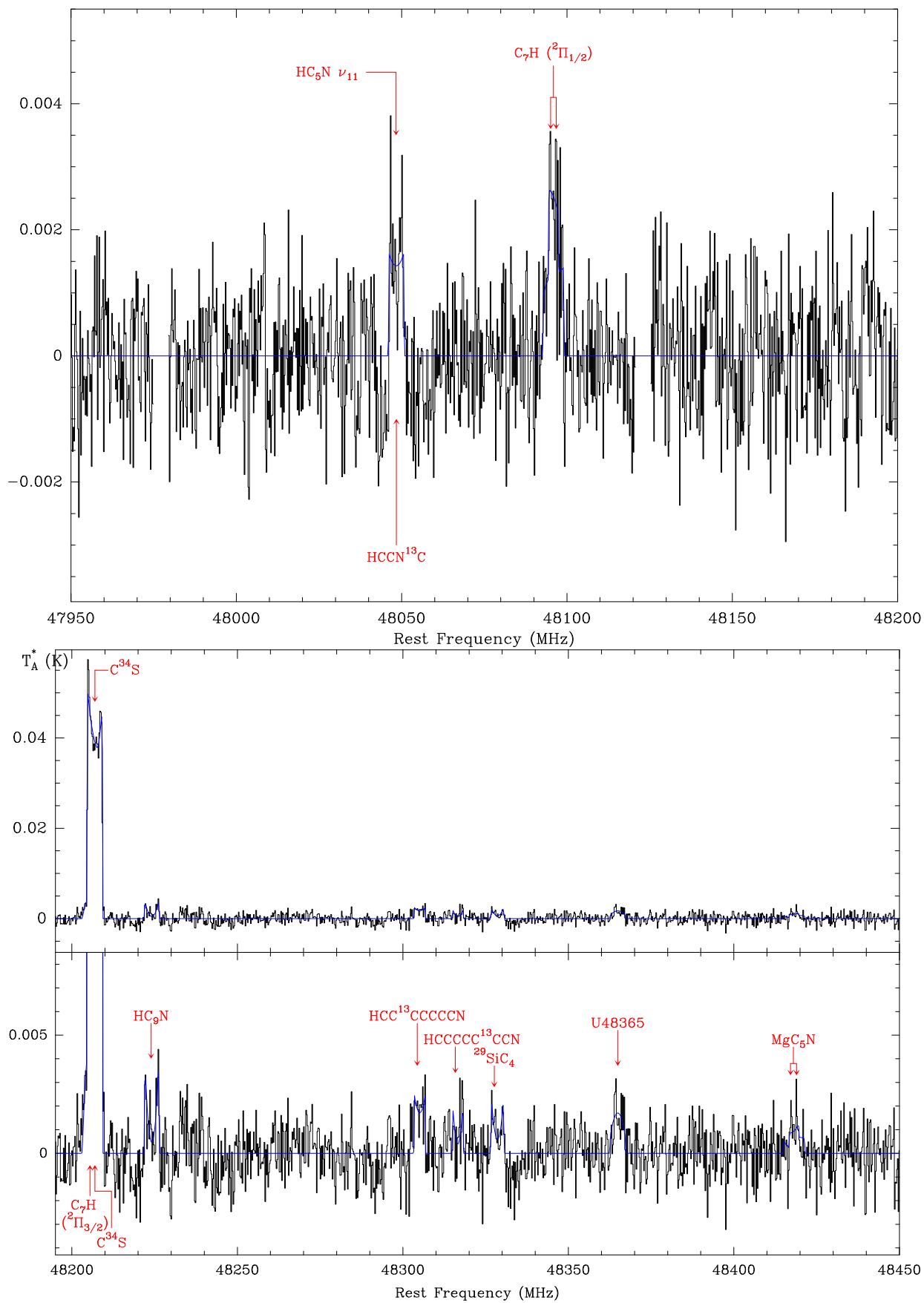
Fig. A.25. IRC+10216 Yebes-40m data, line fits, and labels from 42950 to 43450 GHz.

Fig. A.26. IRC+10216 Yebes-40m data, line fits, and labels from 43450 to 43950 GHz.

Fig. A.27. IRC+10216 Yebes-40m data, line fits, and labels from 43950 to 44450 GHz.

Fig. A.28. IRC+10216 Yebes-40m data, line fits, and labels from 44450 to 44950 GHz.

Fig. A.29. IRC+10216 Yebes-40m data, line fits, and labels from 44950 to 45450 GHz.

Fig. A.30. IRC+10216 Yebes-40m data, line fits, and labels from 45450 to 45950 GHz.

Fig. A.31. IRC+10216 Yebes-40m data, line fits, and labels from 45950 to 46450 GHz.
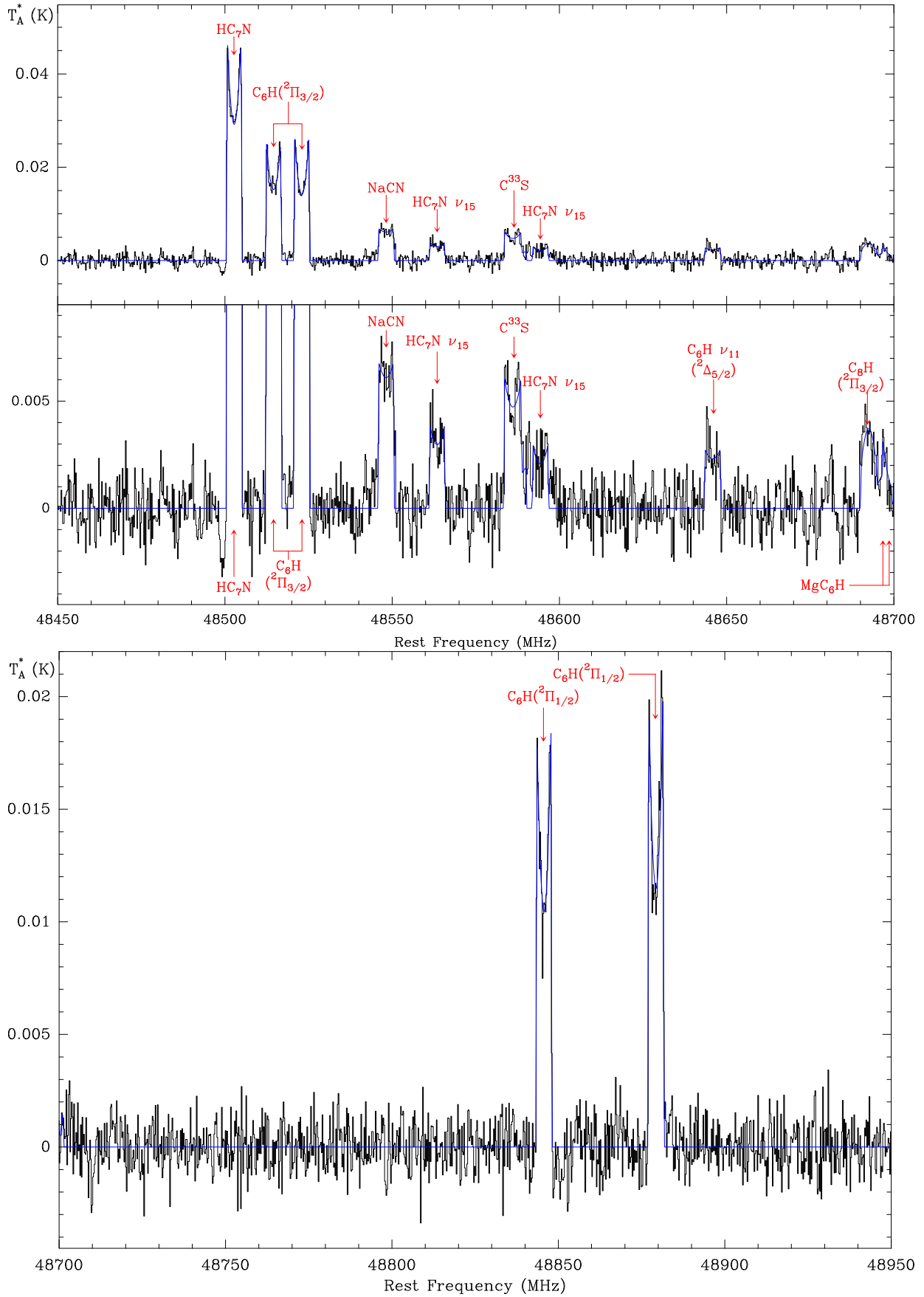
Fig. A.32. IRC+10216 Yebes-40m data, line fits, and labels from 46450 to 46950 GHz.
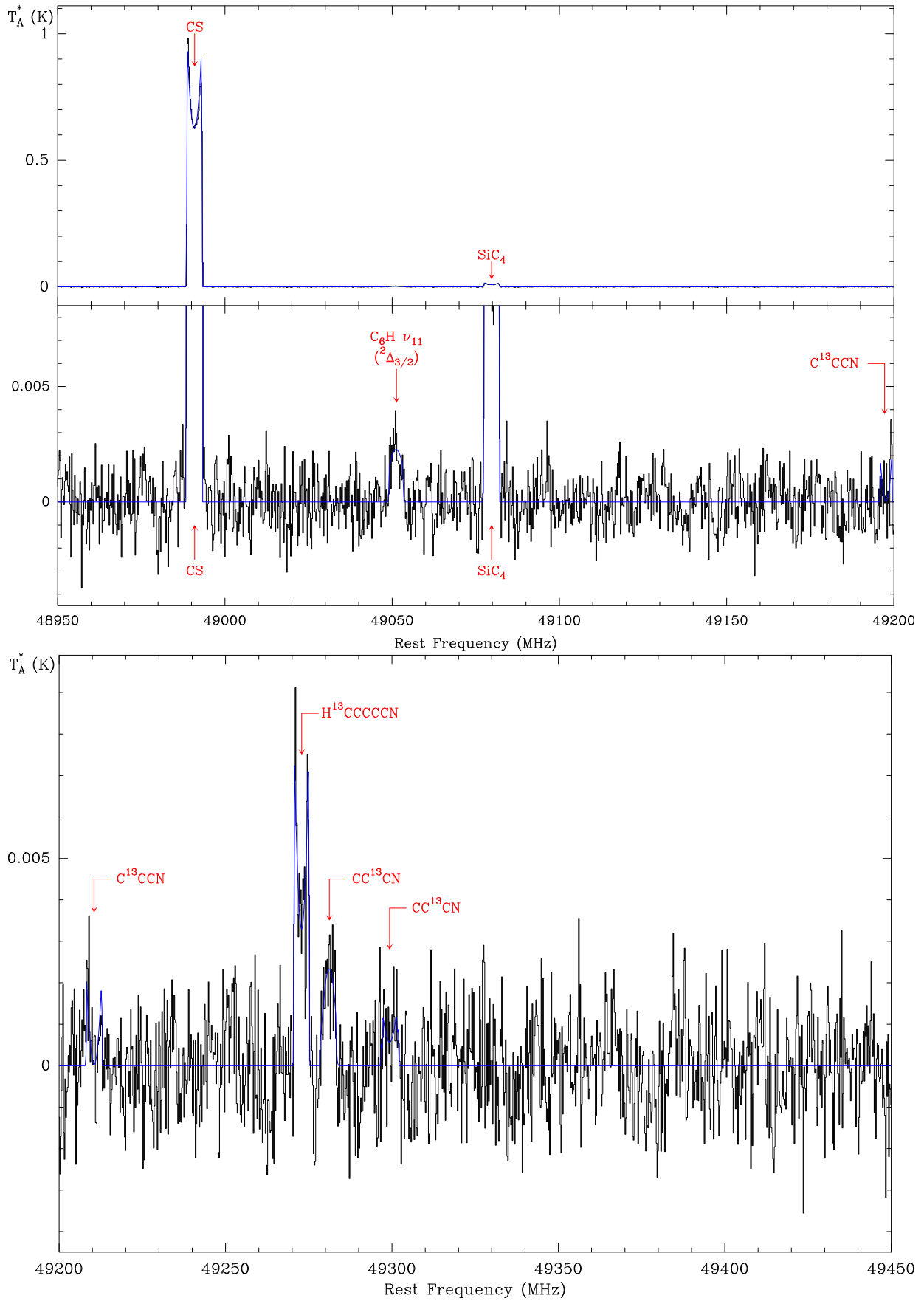
Fig. A.33. IRC+10216 Yebes-40m data, line fits, and labels from 46950 to 47450 GHz.

Fig. A.34. IRC+10216 Yebes-40m data, line fits, and labels from 47450 to 47950 GHz.

Fig. A.35. IRC+10216 Yebes-40m data, line fits, and labels from 47950 to 48450 GHz.

Fig. A.36. IRC+10216 Yebes-40m data, line fits, and labels from 48450 to 48950 GHz.

Fig. A.37. IRC+10216 Yebes-40m data, line fits, and labels from 48950 to 49450 GHz.
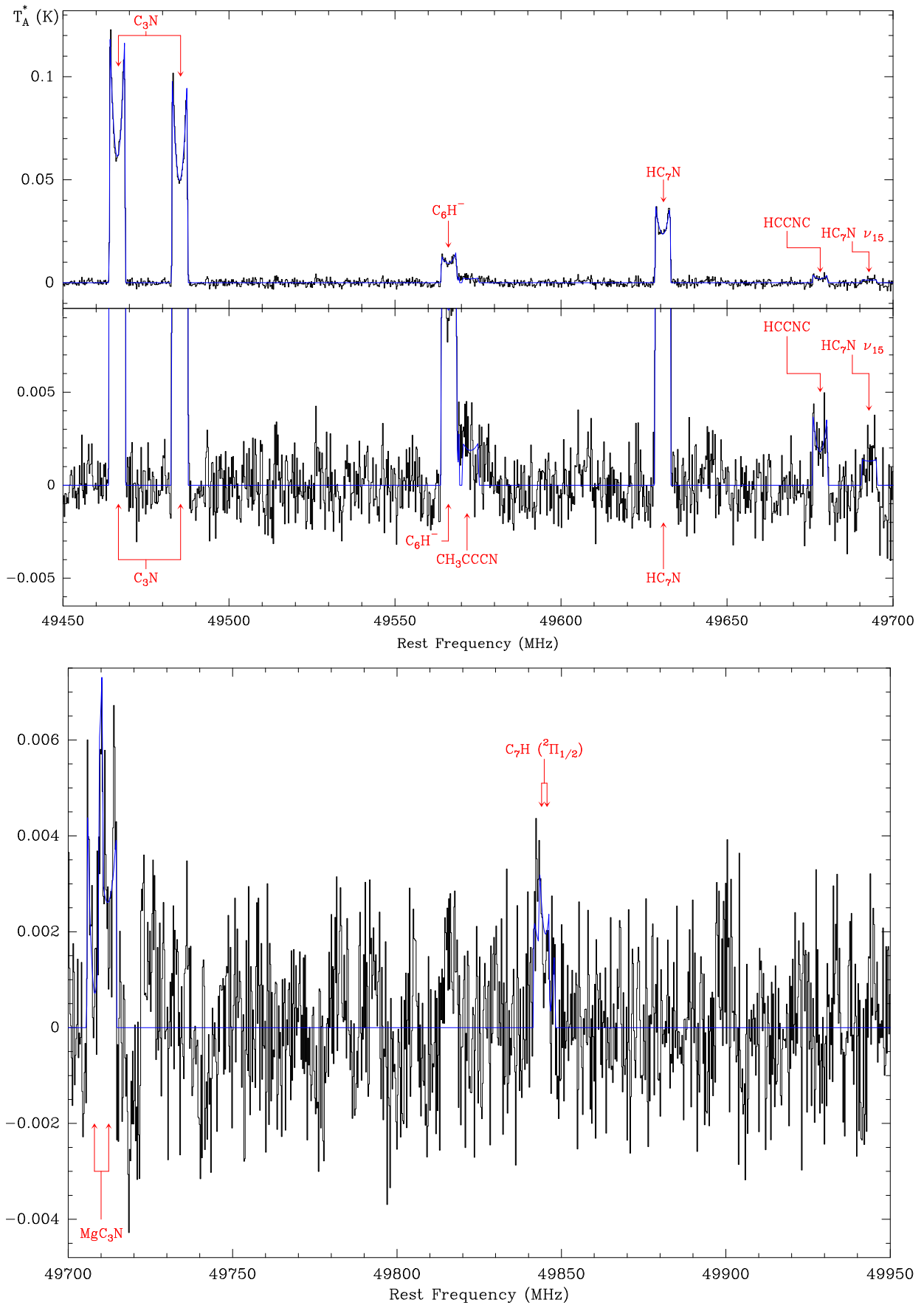
Fig. A.38. IRC+10216 Yebes-40m data, line fits, and labels from 49450 to 49950 GHz.
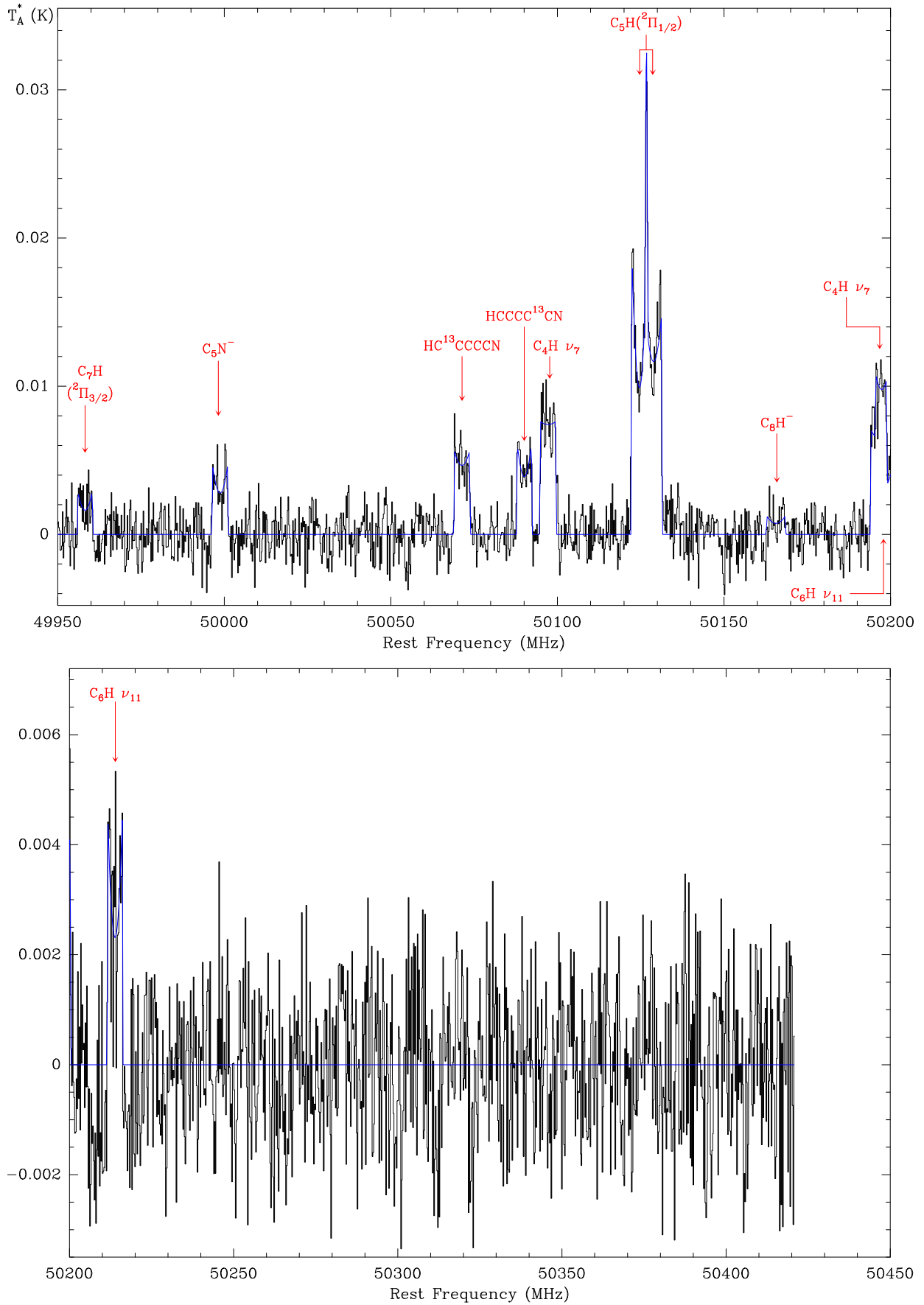
Fig. A.39. IRC+10216 Yebes-40m data, line fits, and labels from 49950 to 50450 GHz.